UNIVERSITY OF KWA-ZULU NATAL

SPATIAL MODULATION: IMPROVING THROUGHPUT OVER NON-CASCADED FADING CHANNELS AND PERFORMANCE ANALYSIS OVER CASCADED FADING CHANNELS

Bhekisizwe Mthethwa

Supervised By: Professor Hongjun Xu

2012

SPATIAL MODULATION: IMPROVING THROUGHPUT OVER NON-CASCADED FADING CHANNELS AND PERFORMANCE ANALYSIS OVER CASCADED FADING CHANNELS

Bhekisizwe Mthethwa

Supervised By: Professor Hongjun Xu

Submitted in fulfillment of the degree of Master of Science in Electronic Engineering,

School of Engineering, University of Kwa-Zulu Natal, Durban, South Africa

October 2012

As the candidate's supervisor I agree to the submission of this dissertation.

Date of Submission: _____

Supervisor: _____

Professor Hongjun Xu

Declaration

I, Bhekisizwe Mthethwa, declare that,

i. The research reported in this dissertation, except where otherwise indicated, is my original work.
ii. This dissertation has not been submitted for any degree or examination at any other university.
iii. This dissertation does not contain other persons' data, pictures, graphs or other information, unless specifically acknowledged as being sourced from other persons.
iv. This dissertation does not contain other persons' writing, unless specifically acknowledged as being sourced from other researchers. Where other written sources have been quoted, then:
    a. Their words have been re-written but the general information attributed to them has been referenced;
    b. Where their exact words have been used, their writing has been placed inside quotation marks, and referenced.
v. Where I have reproduced a publication of which I am an author, co-author or editor, I have indicated in detail which part of the publication was actually written by myself alone and have fully referenced such publications.
vi. This dissertation does not contain text, graphics or tables copied and pasted from the Internet, unless specifically acknowledged, and the source being detailed in the dissertation and in the References sections.

Signed: _____

Acknowledgements

I would like to thank my supervisor, Professor Hongjun Xu, for the academic support and the technical ideas he shared with me while I was carrying out this study. I also thank him for helping me improve my technical writing ability. I would also like to thank the centre of excellence (C.O.E) for their financial support throughout my degree; it would have not been possible to carry out this work without any funding.

I would also like to thank Dr Narushan Pillay, Peter Akuon and Lloyd Blackbeard for reviewing my journal papers for technical quality and ensuring high quality technical language use. Lastly, I would like to thank my girlfriend, Minikazi Mtati, for her financial and moral support while I was carrying out this study. She has been very patient with me coming home late from campus and sometimes working during weekends, this work would have not been produced on time without her selflessness and patience. I thank you all.

Abstract

Small mobile devices which have an ability to access the world wide web (WWW) wirelessly are in demand of late. This demand is attributed to the fact that video and audio streaming are cost effectively accessible via the WWW through wireless fidelity (Wi-Fi). This high demand for cheap real-time multimedia access via Wi-Fi makes it imperative for researchers to develop a wireless local area network (WLAN) standard, such as IEEE (802.11n), that has high data throughput and/or link reliability. The current drawback with the IEEE (802.11n) standard is that it is not power efficient for battery powered small mobile devices because of the high complexity multiple-input-multiple-output (MIMO) scheme implemented within the standard. Spatial modulation (SM) is a recently proposed low complexity MIMO scheme that can achieve high data throughput with good link reliability whilst being power efficient for small mobile devices. This study is aimed at further improving data throughputs of SM and also determining the bit error rate (BER) performance of SM in a city centre environment.

Conventional spatial modulation has been investigated in literature with most research efforts geared towards improving the BER performance and minimizing receiver complexity of the scheme over non-cascaded fading channels. We propose adaptive *M*-ary quadrature amplitude spatial modulation (A-QASM) as a scheme that will improve the average throughput in comparison to conventional spatial modulation given a target BER constraint. The analytical BER lower bound is derived for this proposed scheme and validated by the Monte Carlo simulation results. The simulation results also prove that the average throughput of the proposed scheme (A-QASM) outperforms that of conventional spatial modulation. The definition for the received SNR of the A-QASM scheme is also proposed.

In research literature, conventional spatial modulation has been discussed in depth in non-cascaded wireless fading channels. The performance analysis derived in literature in non-cascaded wireless fading channels; does not apply in predicting the BER performance of a mobile device, using conventional spatial modulation, in an environment where there is signal diffraction (i.e city centre or a forest) which makes the signal susceptible to independent cascaded fading. This study contributes by developing an analytical framework for the BER lower bound of conventional spatial modulation over cascaded fading channels. Simulation results closely agree with the derived theoretical framework.

Table of Contents

List of Figures

List of Tables

List of Acronyms

ACM ..... Adaptive Coded Modulation

A-QASM ..... Adaptive *M*-ary Quadrature Amplitude Spatial Modulation

AM ..... Adaptive Modulation

AWGN ..... Additive White Gaussian Noise

BER ..... Bit Error Rate

CSI ..... Channel State Information

CDF ..... Cumulative Distribution Function

i.i.d ..... Independent and Identically Distributed

IP ..... Internet Protocol

MQAM ..... M-ary Quadrature Amplitude Modulation

MRC ..... Maximal Ratio Combining

ML ..... Maximum Likelihood

MIMO ..... Multiple-Input-Multiple-Output

M S ..... Multi-Stage

OFDM ..... Orthogonal Frequency Division Multiplexing

PER ..... Packet Error Rate

PEP ..... Pairwise Error Probability

PDF ..... Probability Density Function

QoS ..... Quality of Service

SSD ..... Signal Space Diversity

SNR ..... Signal-to-Noise Ratio

SM ..... Spatial Modulation

SEP ..... Symbol Error Probability

TCM .....Trellis Coded Modulation

V-BLAST ..... Vertical Bell Layered Space-Time

WLAN .....Wireless Local Area Network

WWW .....World Wide Web

Wi-Fi .....Wireless Fidelity

Part I

Introduction

1 Introduction

Mobile wireless devices are on high demand due to their convenient ability to allow users to get in touch with their loved ones' via sms or voice calls, to access online emails, chat and to stream videos while mobile. This high demand for wireless mobile devices makes it imperative for wireless engineers and researchers to develop techniques that help improve system throughput and/or link reliability while ensuring that the receiver complexity is kept to a minimum, for practical reasons. The current research literature proposes using MIMO communications as a means to improve system throughput and/or link reliability over a wireless fading channel. The IEEE (802.11n) WLAN standard has implemented MIMO for high data rate transmission and link reliability in Wi-Fi which is a standard implementation in laptops nowadays. Spatial multiplexing schemes, such as vertical bell layered space-time architecture (V-BLAST) [1] are used to divide the data streams into sub-streams for transmission over the MIMO wireless channels. As much as the spatial multiplexing schemes allow for high data rates, they have a drawback of inter-channel interference due to simultaneous transmission of symbols and also require transmit antenna synchronization. These schemes require complicated maximum likelihood detection algorithms [2, 3], which make them power inefficient to implement on small mobile devices which are battery powered. SM [4] is a MIMO scheme proposed to minimize receiver complexity by eliminating inter-channel interference and transmit antenna synchronization, while achieving high data rates. This makes SM attractive for implementation in small mobile devices which are battery powered as lower processing power is used because of lower receiver complexity compared to V-BLAST receivers.

Despite the fact that SM allows for high data transmission over MIMO wireless fading channels, it still leaves room for improvement of throughput. Constant power adaptive modulation [5] is a proposed scheme that adapts the data rate depending on the wireless channel state, in a slowly fading channel, with the objective of improving average throughput subject to a target BER constraint. In adaptive modulation (AM), the received signal-to-noise ratio (SNR) is often used as an indicator of channel state [5] and is used to select the most optimal data rate for transmission over a particular wireless channel state. The idea is that, as the channel state varies stochastically, in a quasi-static fashion [5], M-ary quadrature amplitude modulation (MQAM) modulation orders (discrete data rates) are chosen in such a way as to optimize spectral

efficiency subject to a target BER constraint. When the exceptional case occurs of a very poor channel state, no data transmission occurs in order to avoid deep fading. AM is particularly advantageous over the conventional single data rate transmission, as the highest possible data rates are always chosen to optimize the spectral efficiency of the wireless system. The conventional single data rate transmission has no choice but to transmit at the same data rate even if the channel state allows for higher data rate transmission over the wireless fading channel. This is an obvious loss of system throughput as more data, on average, could be sent per given time. We employ constant power AM with SM to improve the average throughput performance of SM given a target BER constraint. This adaptive rate scheme will ensure that higher data rates are achievable in small mobile devices and thus it will improve, for instance, the delay performance of video-streaming to these wireless devices.

SM has been studied in detail over non-cascaded wireless fading channels with a Rayleigh distributed fading gain, which is an accurate model for severe short-term fading channels [9], [20], [21]. The analytical BER performance results of SM derived under the short-term fading channel model cannot be used to predict BER performances in long-term and mixed fading wireless environments. The analytical BER of SM derived in literature cannot also be used to predict the BER performance of a wireless mobile device used in a forest or city centre environment. This is as a result of diffraction, for example by street corners in a city centre, of the radio signal during propagation to the base station or to another user. The diffraction of the signal increases the likelihood of the radio signal to experience independent cascaded fading. The BER performance of SM over such a cascaded wireless fading channel is expected to be worse relative to that of the non-cascaded fading channel, hence new analytical BER bounds need to be derived. We derive an approximate BER lower bound for SM over independent and identically distributed (i.i.d) wireless cascaded fading channels. This is particularly useful as a benchmark for research work involved in improving BER performance of mobile devices using SM in a city centre environment.

1.1 Spatial modulation

Spatial modulation [4] is a recently proposed MIMO scheme that eliminates inter-channel interference and the need for transmit antenna synchronization, thus it is regarded as a low

complexity MIMO scheme. As a result of its low complexity relative to MIMO schemes like V-BLAST [1], it is a promising MIMO scheme for implementation in small mobile devices.

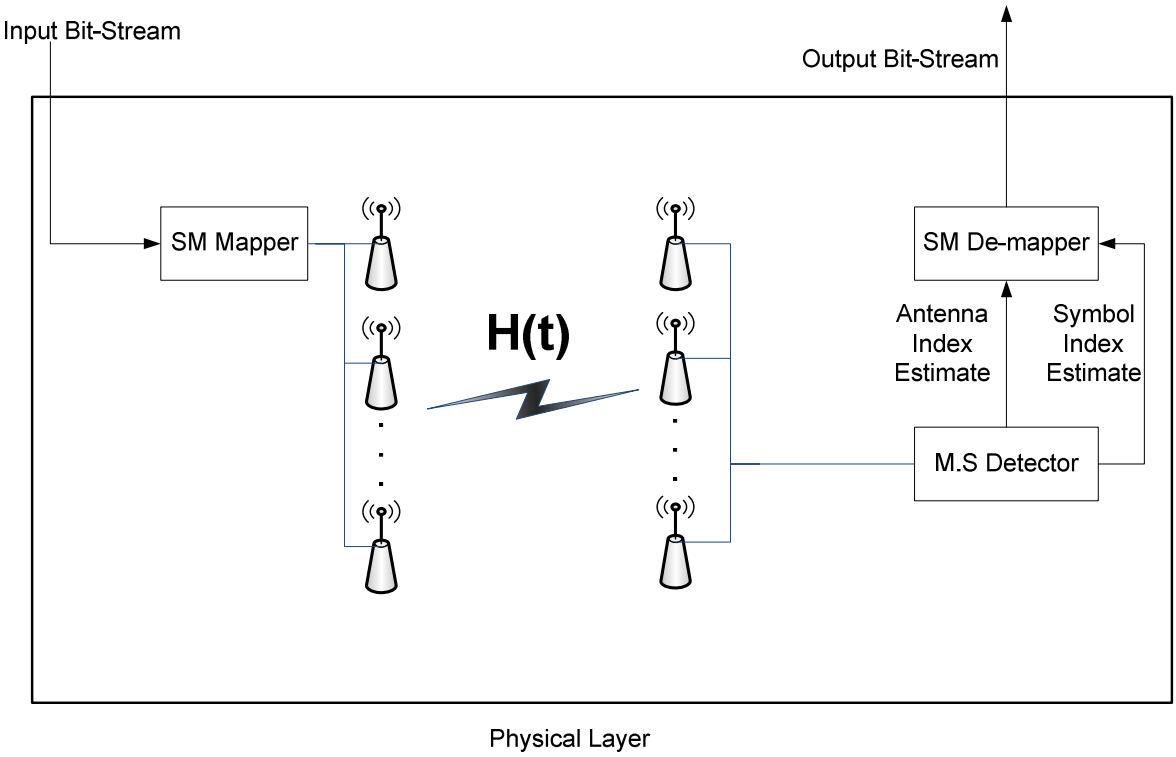

Fig. 1.1 System model of spatial modulation [4]

Fig. 1.1 shows the system model of an $L_t \times L_r$ SM scheme where L_t and L_r are defined as the number of transmit and receive antennae, respectively. SM eliminates inter-channel interference by transmitting using only one transmit antenna at a time. This method of transmission also eliminates the need for transmit antenna synchronization as data streams are not sent on all transmit antennae simultaneously. As a result of this, receiver complexity is reduced by ~90% relative to V-BLAST receiver complexity [22] at the same spectral efficiency. From Fig. 1.1, SM receives a random input bit stream that enters the SM mapper. This mapper maps r bits, where $r = \log_2(L_t M)$ and M is the MQAM signal constellation size, to a constellation vector $\boldsymbol{x} = [x_1\ x_2\ \ldots x_{L_t}]^T$ and it is assumed that the average power is unity. Since in SM only one transmit antenna is active at a given time, it implies that only one element of the constellation

vector $\boldsymbol{x}$ is non-zero, since the other transmit antennae are dormant. SM exploits the ability of the transmit antenna index to carry extra information by assigning random data bits to transmit antenna indices. After SM transmission has occurred over $L_r \times L_t$ wireless fading channels $\boldsymbol{H}(t)$ with additive white Gaussian noise (AWGN), the receiver node uses maximal ratio combining (MRC) as a diversity combiner of choice and an SM detection scheme that estimates the transmitted symbol and the active transmit antenna index. Based on the estimated symbol and transmit antenna index, the SM-demapper decodes the transmitted bit stream. Various SM detection schemes are used in literature to detect the transmitted symbol and active transmit antenna index. Since this MIMO scheme is a promising scheme to be implemented in small mobile devices, receiver complexity is an interesting research area with the aim to minimize receiver complexity of SM while maintaining the BER performance. The next sub-section discusses various low-complexity SM detection schemes.

Spatial modulation detection schemes

The main objective of SM is to provide a high data rate MIMO scheme similar to V-BLAST but with a much lower complexity, such that practical implementation in small mobile devices is feasible. This is advantageous as high data rates will become achievable in small mobile devices as a result of the practically feasible low complexity SM scheme. Researchers have thus gained interest in minimizing receiver complexity of SM while maintaining the BER performance. In [22] SM is proposed with a low complexity sub-optimal detection scheme (for estimating the transmitted symbol and the active transmit antenna index) that has a poor BER performance relative to the maximum likelihood (ML) based optimal detection scheme proposed by [23]. Despite its poor BER performance, it has an advantage of lower receiver complexity relative to an ML-based optimal detector. In [18] a multi-stage SM detection scheme is proposed which reduces receiver complexity of SM relative to the ML-based optimal detection scheme whilst achieving similar BER performance. Receiver complexity is further reduced by [19] who simplifies the ML-based optimal detection scheme proposed by [23]. [19] exposes the inefficiency in searching for the transmit antenna index and transmitted symbol pair among all possible $L_t M$ pairs as stipulated in the ML-based optimal detection scheme. The author in [19] then proposes a simplified ML-based detection scheme that first searches for pairs of transmit antenna index and transmitted symbol in level-one subsets, which the transmitted signal most

probably belongs to, and then secondly searches for these pairs in level-two subsets among those pairs in level-one subsets. The author concludes that the receiver complexity of the proposed simplified ML-based optimal detector is much lower than that of the ML-based optimal detector proposed by [23]. The BER performance is maintained by this new low complexity SM detection scheme until a BER performance of 10^{-6}. In this study, multi-stage detection is used in Paper A and ML-based optimal detection is used in Paper B.

1.2 Adaptive Modulation

The spectral efficiency of a fading channel varies with the change in wireless channel state. The wireless channel state is estimated by the received SNR. It is known that as the received SNR increases, the spectral efficiency of a wireless fading channel also increases [6] and thus higher data rates can be achieved over the wireless channel while meeting target BER constraints. The same can be concluded if the received SNR decreases, the spectral efficiency of the wireless fading channel also decreases and hence the maximum data rate that can be supported over the wireless channel drops for a given target BER. Conventional single data rate transmission under-utilizes the spectral efficiency of a wireless fading channel as the fixed data rate is designed by taking into consideration the worst case channel conditions [6]. AM improves the utilization of the spectral efficiency, by selecting the most optimal transmission data rates based on the wireless channel quality, subject to a target BER constraint.

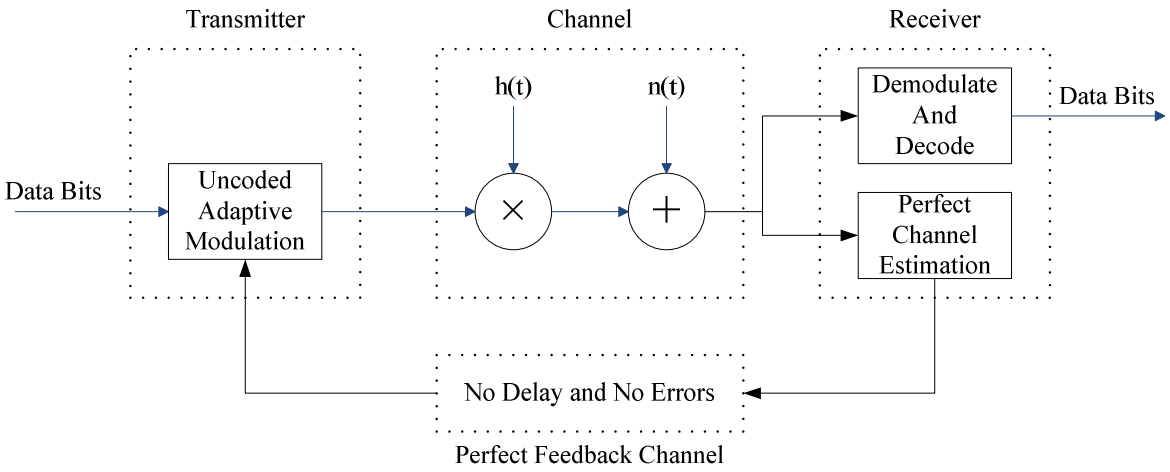

Fig. 1.2 Un-coded adaptive modulation system model adopted from [8]

Fig. 1.2 exhibits a typical adaptive rate transmission scheme over a quasi-static frequency flat fading channel $h(t)$. Before transmission occurs, and assuming the channel state information (CSI) is perfectly estimated during the guard period of the previously transmitted frame, the received SNR is compared to the AM switching levels that are determined in such a way as to maximize the average system throughput while meeting a target BER constraint. After comparing the received SNR to the AM switching levels, the modulation index is determined based on which AM switching level range (SNR bin) the received SNR lies in. This modulation index is fed back to the transmitter via a perfect feedback channel and is used to adapt the MQAM transmission modulation order based on CSI in such a way as to optimize the average throughput of the system. A frame is thus transmitted with an optimal data rate for that particular wireless fading channel quality, and the data rate is adapted on a frame by frame basis in order to mitigate fading. The AM scheme shown in Fig. 1.2 is a constant power un-coded AM scheme. Other AM schemes exist that further improve average throughput/spectral efficiency; these will be discussed in the next sub-section.

Adaptive modulation schemes

Adaptive coded modulation (ACM) is discussed in [8] where coset codes are applied to AM in order to improve the BER performance of AM. The advantage of the ACM system is that the coding and modulation design are separable and hence the data throughput can be maximized without affecting the coding gain achieved by the coset codes. This implies that higher data rates can be achieved by ACM relative to un-coded AM for the same wireless channel quality.

Goldsmith et al [6] propose an adaptive rate and power scheme to improve spectral efficiency/throughput subject to average power and BER constraints. Their scheme adapts transmit power in a "water-filling" fashion in order to maximize spectral efficiency. When the received SNR or channel quality is good, the transmit power is increased. If the channel conditions deteriorate, the transmit power is reduced. When the channel quality drops below the cutoff threshold, during deep fading, no power is allocated for transmission. This scheme achieves within 1-2 dB of the maximum spectral efficiency and also proves to be power efficient relative to variable power fixed-rate transmission by 5-10 dB. The adaptive power and rate scheme is also shown to have a power saving of up to 20 dB relative to non-adaptive schemes. In

[6] it is mentioned that a variable power fixed-rate (channel inversion) scheme has the ability to maintain a constant received SNR and hence can support a fixed data rate. Such a scheme is shown to be power inefficient as it is not restricted from compensating transmit power during deep fading. However, [7] shows that this scheme can be useful when transmitting data services with stringent quality of service (QoS) requirements (e.g real-time multimedia applications) over a wireless fading channel, as fixed-data rate transmission will occur regardless of the quality of the wireless channel. Transmission will also occur during deep fading; hence data packets at the data link layer buffer will always be serviced so as to meet the stringent QoS requirements.

Due to the high throughput capabilities AM can offer, we therefore apply AM to SM in order to achieve high data rates in small mobile devices. We choose un-coded AM because of its simplicity and mainly as a proof of concept. Hence, the proposed A-QASM scheme in Paper A serves as a benchmark for comparison purposes in future studies. Other AM schemes, as already discussed, can be applied to SM in future studies to further improve throughput and/or minimize power loss.

1.3 Wireless fading channels

Since there is a high demand for mobile devices which users can use in any wireless environment, it is important to discuss the different fading channel environments mobile devices can be used in. Based on these fading channel environments, different channel models are applied to different wireless environments in order for it to be possible to accurately estimate the BER performance of any wireless scheme over different terrain. The different wireless environments are discussed in this section.

When a mobile device transmits signals, the signals spread out in all directions taking different paths to the receiver node. As these signals travel through the wireless medium, they experience reflections from trees, mountains, and buildings. This causes the signals to arrive out of phase with each other when the receiver node receives the signals. The signals at the receiver are superimposed and experience signal degradation due to constructive and destructive interference. This signal degradation is called multipath fading [24]. Different wireless environments give rise to different fading intensities and statistical distributions governing their stochastic fading gain. Fading channels can be grouped into four different categories namely: short-term, long-term,

mixed and cascaded fading. These fading groups or categories exist in different geographical locations, sizes and different terrains; hence it is important to determine the channel model and error performance of a wireless scheme over different terrains.

It is discussed in literature [9], [20], [21] that the fading gain in a small geographical area, which is hundreds of wavelengths in dimension, is Rayleigh distributed. This small geographical area experiences what is called short-term fading due to the short distance point-point communications involved. Long-term fading occurs in larger geographical areas where long distance communication occurs and the fading gain is found via experiments to be lognormally distributed [25]. It is possible for wireless channels to experience mixed fading where short-term and long-term fading coexist. Various fading channel gain models are proposed by [10-12], for mixed fading environments. These proposed models are the Suzuki, Rice-lognormal and Rayleigh-lognormal distributions. The other fading channel model of interest is that of independent cascaded fading. This arises as a result of signal diffraction of the radio signal during propagation. This phenomenon of radio signal diffraction occurs on street corners in city centres and even in a forest environment [13]. As the signal experiences diffraction, independent fading scenarios occur and thus a multiplicative/cascaded fading channel starts to exist between two communicating points. Various cascaded fading channel models exist for different terrains where radio signal diffraction is common and they are: cascaded Rayleigh [14], cascaded Nakagami [15] and cascaded generalized-K [16] fading models. In [17], signal space diversity (SSD) is applied over multiplicative/cascaded fading channels and the fading channel model used is the cascaded Nakagami. This is an example of growing interest amongst researchers for the need to analyze the performance of wireless schemes over cascaded fading channels.

In this dissertation, we choose to analyze the error performance of SM over a city centre environment as it is a common place for urban dwellers. This city centre environment, with its many street corners, has a very high likelihood of allowing independent cascaded fading to occur as a result of multiple diffraction of the radio signal. For our study, we assume that for each path the radio signal takes, after diffraction, the signal experiences short-term fading with a fading gain that is Rayleigh distributed. We therefore analyze the error performance of SM over cascaded wireless channels with i.i.d Rayleigh distributed fading gains.

2 Motivation and Research Objective

SM is discussed in depth in literature, together with schemes to improve the error performance of SM over a fading channel. Receiver complexity is also discussed and strategies are devised to minimize the complexity for practical implementation and speed [18, 19]. However, the literature shows that there is little research already done towards improving average throughput in SM. This inspires us to study A-QASM in order to improve the average throughput of SM over wireless complex fading channels subject to a target BER constraint.

Mobile devices experience fading in various environments. Some environments give rise to short-term fading, long-term fading, mixed fading or cascaded fading. Since SM is a low complexity MIMO scheme, it is an attractive scheme for practical implementation in small mobile devices. Wireless mobile device users do not restrict their movements to environments that only experience short term fading. A city centre is a frequent location for urban dwellers and the use of wireless mobile devices in such an environment is inevitable. The city centre wireless environment is likely to follow a cascaded fading channel model due to diffraction from street corners [13], hence conventional short-term non-cascaded fading models cannot be applied in that environment. Research on SM has been largely done on short-term fading environments (i.e channel gains modeled by the Rayleigh distribution). It is apparent that more research work needs to be done to cater for the non-short-term fading environments. This motivates us to study the BER performance of SM over cascaded fading channels.

3 Contributions of Included Papers

The contributions of this dissertation are presented in two journal papers in Section II and Section III concludes the dissertation.

3.1 Paper A

B.M. Mthethwa, H. Xu, "Adaptive M-ary Quadrature Amplitude Spatial Modulation", *IET Communications*, Volume 6, Issue 18, pp. 3098-3108, December 2012.

In Paper A, A-QASM is a scheme proposed in this study to improve average throughput of conventional SM. Two definitions for the received SNR of an A-QASM scheme are also proposed. Using either definition of the received SNR, it is shown via Monte Carlo simulations that they yield similar A-QASM BER and throughput performance, under the perfect channel state information (CSI) assumption. The A-QASM analytical BER lower bound is also derived and validated via simulations.

3.2 Paper B

B.M. Mthethwa, H. Xu, "Spatial Modulation over K Multiplicative Complex Fading Wireless Channels", [Fully Accepted for publication in IET Communications Journal], 2013.

In Paper B, SM is implemented over K cascaded/multiplicative complex fading wireless channels. The analytical BER lower bound approximation is derived and validated via simulations for different K values and MIMO configuration. The BER lower bound is only shown to be applicable where $M \gg L_t$. We also propose an algorithm for determining an approximate distribution function, together with its parameters, for a stochastic variable with an unknown distribution. The approximate distribution and its parameters are validated as an appropriate fit by a goodness of fit test at the 5% significance level.

4 Future Work

The packet error rate (PER) of SM is an important QoS metric to be derived for the use in improving the delay performance at the data link layer, using cross layer design, of an internet protocol (IP) network subject to target PER constraint. Further, A-QASM error probability and throughput performance evaluations need to be done for both proposed received SNR definitions in an environment with imperfect CSI. It is also vital for future research work to define exact A-QASM received SNR as opposed to an approximate definition that includes the laborious method of finding suitable scaling factors in order to estimate the actual received SNR. In this study, un-coded constant power adaptive modulation is applied to an SM scheme to improve throughput. Alternatively, an adaptive power and rate technique [6] can be applied to SM to improve throughput and energy efficiency, or a coded adaptive rate technique [8] can be applied to an SM scheme to improve throughput.

The derived BER of SM over K cascaded/multiplicative fading channels is not generic in this dissertation. It remains an open problem to derive an analytical BER of SM in wireless cascaded fading channels with a generic fading gain distribution (e.g Nakagami-m) for each K independent cascaded wireless path. It is also interesting to find a closed form expression for the average pairwise error probability (PEP) as opposed to the approximation presented in this dissertation.

5 References

[1]. P. Wolniansky, G. Foschini, G. Golden and R. Valenzuela, "V-BLAST: An Architecture for Realizing very High Data Rates over the Rich-Scattering Wireless Channel", in *Proc URSI Int. Symp. on Signals ,Systems and Electronics (ISSSE '98.)*, Pisa, pp. 295–300, 1998.

[2]. Goldsmith, A., Jafar, S., Jindal, N., Vishwanath, S, "Capacity limits of MIMO channels", *IEEE J. Sel. Areas Commun.*, pp. 684–702, 2003.

[3]. Damen, M., Abdi, A., Kaveh, M. "On the effect of correlated fading on several space-time coding and detection schemes", *Proc. IEEE Vehicular Technol. Conf.*, Atlantic City, NJ, pp. 13–16, 2001.

[4]. R.Y. Mesleh, H. Haas, C.W. Ahn, S. Yun, "Spatial modulation-a new low complexity spectral efficiency enhancing technique", *First international conference on communications and networking in China*, 2006.

[5]. M. S. Alouini and A. J. Goldsmith, "Adaptive modulation over Nakagami fading channels", *J. Wireless Commun.*, vol. 13, no. 1–2, pp.119–143, 2000.

[6]. A.J. Goldsmith, Soon-Ghee Chua, "Variable-rate variable-power MQAM for fading channels", *IEEE Transactions on Communications*, Vol. 45, no. 10, pp. 1218-1230, 1997.

[7]. J. Tang, X. Zhang, "Quality-of-Service driven Power and Rate adaptation for multichannel communications over wireless links", *IEEE Transactions on Wireless Communications*, Vol. 6, no. 12, pp. 4349-4360, 2007.

[8]. A.J. Goldsmith, Soon-Ghee Chua, "Adaptive coded modulation for fading channels", *IEEE Transactions on communications*, Vol. 46, no. 5, pp. 595 – 602, 1998.

[9]. H. F. Schmid, "A prediction model for multipath propagation of pulse signals at VHF and UHF over irregular terrain", *IEEE Trans. Antennas Propagat*., Vol. AP-18, pp. 253-258, 1970.

[10]. H. Suzuki, “A statistical model for urban radio propagation”, *IEEE Transactions on Communications*, Vol. Com-25, no. 7, pp. 673-680, 1977.

[11]. F. Vatalaro, G.E. Corazza, “Probability of error and outage in a Rice-lognormal channel for Terrestrial and Satellite personal communications”, *IEEE Transactions on communications*, Vol. 44, no. 8, pp. 921-924, 1996.

[12]. F. Hansen, F.I. Meno, “Mobile fading-Rayleigh and lognormal superimposed”, *IEEE Transactions on Vehicular Technology*, Vol. VT-26, no. 4, pp. 332-335, 1977.

[13]. V. Erceg, S.J. Fortune, J. Ling, A.J. Rustako, R.A. Valenzuela, “Comparisons of a computer based propagation prediction tool with experimental data collected in urban microcellular environments”, *IEEE Journal on selected areas in communications*, Vol. 15, no. 4, pp. 667-684, 1997.

[14]. J. Salo, H.M. El-Sallabi, P. Vainikainen, “The distribution of the product of independent Rayleigh Random Variables”, *IEEE Transactions on antennas and propagation*, Vol. 54, no. 2, pp. 639-643, 2006.

[15]. G.K. Karagiannidis, N.C. Sagias, P.T. Mathiopoulos, “N*Nakagami: A Novel Stochastic Model for cascaded fading channels*”, IEEE Trans. on Comms,* Vol. 55, no. 8, pp. 1453-1458, 2007.

[16]. K. Peppas, F. Lazarakis, A. Alexandridis, K. Dangakis, “Cascaded generalized-K fading channel”, *IET proceedings Communications*, Vol. 4, Issue 1, pp.116-124, 2010.

[17]. N.H. Tran, H.H. Nguyen, T. Le-Ngoc, “Application of signal space diversity over multiplicative fading channels”, *IEEE Signal processing letters*, Vol. 16, no. 3, pp. 204-207, 2009.

[18]. N. R. Naidoo, H. Xu and T. Quazi, "Spatial Modulation: Optimal Detector Asymptotic Performance and Multiple-stage Detection", *IET proceedings Communications ,* Vol. 5, no. 10*,* pp. 1368-1376, 2011.

[19]. H. Xu, "Simplified ML Based Detection Schemes for M-QAM Spatial Modulation Trellis coded spatial modulation", *IET proceedings Communications*, Vol. 6, Issue 11, pp. 1356-1363, 2012

[20]. R. H. Clarke, "A statistical theory of mobile-radio reception", *Bell Syst. Tech. J.*, Vol. 47, pp. 957-1000, 1968.

[21]. J. J. Egli, "Radio propagation above 40 mc over irregular terrain", *Proc. IRE*, Vol. 45, pp. 1383-1391, 1957.

[22]. R. Y. Mesleh, H. Haas, S. Sinanovi´c, C. Wook Ahn, S. Yun, "Spatial Modulation", *IEEE Transactions on Vehicular technology*, Vol.57, no. 4, pp. 2228-2241, 2008.

[23]. J. Jeganathan, A. Ghrayeb, L. Szczecinski, "Spatial modulation: optimal detection and performance analysis", *IEEE Communications Letters*, Vol. 12, no. 8, pp. 545-547, 2008.

[24]. G. L. Stuber, "Mobile Communication*"*, 2nd edition. Norwell, MA: Kluwer, 2003.

[25]. G. L. Turin, F. D. Clapp, T. L. Johnston, S. B. Fine, and D. Lavry, "A statistical model of urban multipath propagation," *IEEE Transactions on Vehicular Technology*, Vol. VT-21, pp. 19–335, 1972.

Part II

Included Papers

Paper A

Adaptive *M*-ary Quadrature Amplitude Spatial Modulation

B.M. Mthethwa, and H. Xu

IET Communications, Volume 6, Issue 18, pp. 3098-3108,
December 2012

Abstract

Spatial modulation (SM) is a low complexity, highly spectral efficient Multiple-Input-Multiple-Output (MIMO) scheme that has been proposed in literature. We apply adaptive modulation to conventional SM in order to maximize the average throughput of the scheme. For this to be possible, the equivalent received signal-to-noise ratio (SNR) needs to be defined and is done so via two proposed approaches: using the first order statistics SNR and using the average statistics SNR. Average theoretical bit error rate (BER) bounds are derived for both of these SNR approaches. Also, adaptive *M*-ary quadrature amplitude spatial modulation (A-QASM) switching levels are determined to maximize the throughput whilst meeting the average target BER. The Monte-Carlo simulation results successfully validate the derived theoretical BER bounds and also prove that the average throughput is improved in comparison to conventional SM. The two proposed definitions for the equivalent received SNR are confirmed to yield comparable BER and throughput performances via simulations, implying that the equivalent received SNR can be defined using either approach.

1 Introduction

With a high demand for wireless products, it becomes imperative for next generation wireless solutions to provide higher data rates and link reliability than previous generations. MIMO schemes are a good solution to providing high data rates and link reliability. Spatial modulation (SM), henceforth referred to as conventional SM, was proposed by Mesleh et al [1-2] as a MIMO scheme which in comparison to MIMO V-BLAST transmission [3], eliminates the need for transmit antenna synchronization and eliminates inter-channel interference. SM transmits a symbol using a single active transmit antenna for each time slot, effectively suppressing inter-channel interference. Additional data is conveyed by the spatial position of the active transmit antenna, selected by mapping information to a spatial constellation. The latest research achievements and some open issues of SM were recently summarized in [4].

For the detection of conventional SM, a maximum likelihood (ML) based detector was developed in [5] and sub-optimal and multi-stage detection were proposed in [6]. Maximal Ratio Combining (MRC) based SM detection was found to be sub-optimal and hence an ML- based optimal SM detector was proposed by [5], a simplified ML detector was proposed in [7] and very recently, signal vector based detection was developed in [8].

Based on conventional SM, other novel SM schemes have been developed. Some examples are: (i) Trellis coded modulation (TCM) is applied to the antenna constellation points of SM in order to improve performance over spatially correlated channels in [9]; (ii) A soft-output ML detector for SM orthogonal frequency division multiplexing (OFDM) systems is introduced and shown to outperform the conventional hard decision based SM detector in [10]; (iii) Spatial modulation with trellis coding is investigated in [11] and is shown to improve the BER performance relative to coded V-BLAST; (iv) space shift keying is proposed to avoid any form of conventional modulation, trading receiver complexity for achievable rates [12]; and (v) an adaptive spatial modulation scheme is investigated in [13].

In [13], adaptive modulation is based on a modulation order selection algorithm which minimizes the conditional pairwise error probability for each channel realization. The algorithm in [13] is less complex in comparison to the V-BLAST adaptive modulation system that is proposed in [14], but can achieve similar BER performance whilst maintaining a common target average transmission bit rate. However, the authors in [14] did not discuss the issue of adaptive

modulation in an SM scheme as a means to improve average data throughput (bits/transmission). With this in mind, a scheme deemed A-QASM is proposed to improve average throughput in comparison to conventional SM. To derive theoretical average BER bounds for A-QASM, the equivalent received SNR is defined. Two approaches, the first order statistical SNR and the average statistics SNR, are proposed to define the equivalent received SNR. The two approaches are compared to see if they are similar in performance in terms of average BER and average throughput.

The paper is organized in the following way: Section 2 discusses the system model of A-QASM; Section 3 discusses the statistics of the received SNR for the proposed A-QASM scheme; Section 4 derives theoretical BER bounds for A-QASM; Section 5 validates the theoretical framework derived in Section 4 and discusses the difference in average throughput performance between conventional spatial modulation and adaptive spatial modulation; lastly Section 6 draws the conclusion of the paper.

2 System Model

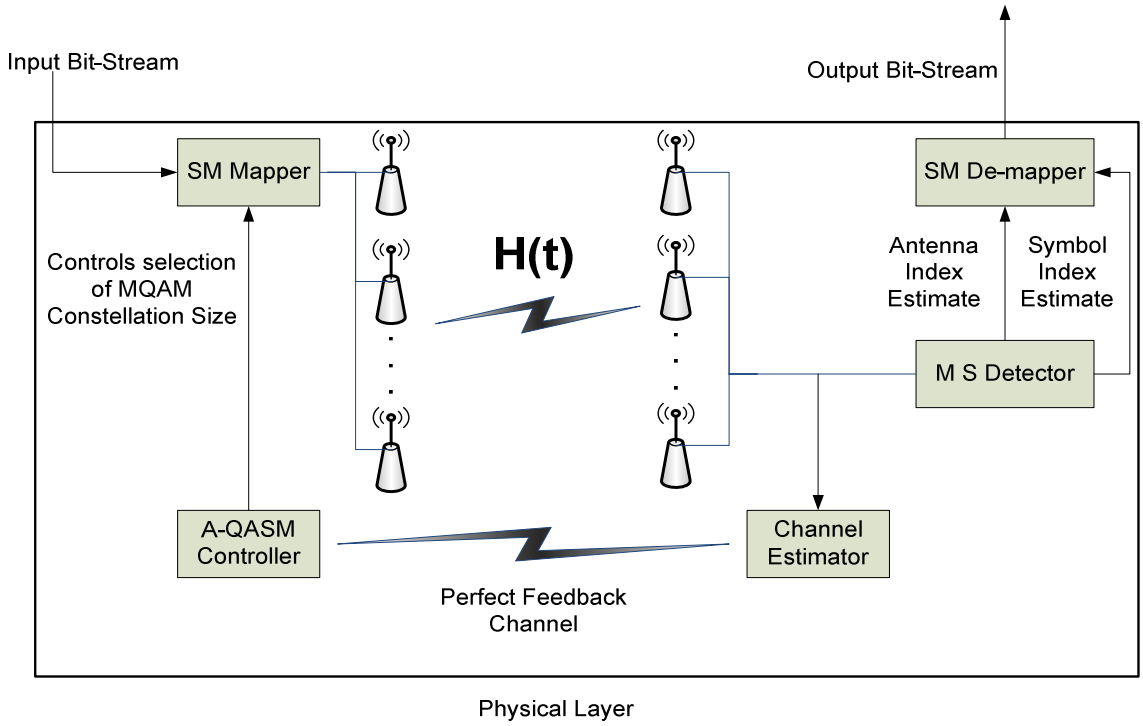

Fig. A.1 System model of A-QASM

2.1 System Model

We consider the $L_t \times L_r$ A-QASM scheme shown in Fig. A.1: L_t and L_r are respectively the number of transmit and the number of receive antennas in the MIMO configuration. The proposed A-QASM scheme has an A-QASM controller that adapts the size, *M*, of the M-QAM signal constellation in order to optimise the spectral efficiency for a number of particular channel states. As in [14], it is assumed that the channel state information (CSI) for an entire frame is perfectly estimated in the guard period of each frame at the receiver and that the CSI is fed back to the transmitter over a perfect feedback channel. Based on the received CSI which is fed back, the transmitter selects an M-QAM signal constellation size which is then used in the transmission of input information using spatial modulation [2]. The wireless channel is modelled and denoted by an $L_r \times L_t$ complex fading channel $\boldsymbol{H}$ with L_r dimensional additive white Gaussian noise (AWGN) elements $\boldsymbol{n}=[n_1\ n_2 \ldots n_{L_r}]^T$. Both $\boldsymbol{H}$ and $\boldsymbol{n}$ have i.i.d random elements which are distributed according to the complex Gaussian *CN* (0,1) [6]:thus, the channel gain for each path

is Rayleigh distributed. It is assumed that the channel is time varying in a quasi-static fading fashion, such that the channel gain on each path varies on a frame by frame basis without any correlation between frames. However, the channel gain remains constant per frame. At the receiver, MRC diversity combining is used in conjunction with multi-stage (M S) detection for optimal BER performance and low receiver complexity [6]. The received signal vector $\boldsymbol{y}$ at the receiver is given by [6]

$$\boldsymbol{y} = \sqrt{\bar{\gamma}}\boldsymbol{H}\boldsymbol{x}_{jq} + \boldsymbol{n} \tag{A.1}$$

where $\boldsymbol{y} = \left[y_1\, y_2 \ldots y_{L_r}\right]^T$ represents the received signal vector, $\bar{\gamma}$ is the average received SNR at each receive antenna, $\boldsymbol{x}_{jq}$ is the symbol vector transmitting the q^{th} M-QAM symbol from transmit antenna j, $j \in [1{:}\,L_t]$, $q \in [1{:}\,M]$ and $[\cdot]^T$ is the vector transpose function.

2.2 M-QAM based link adaptation

Here, we consider an adaptive M-QAM system without coding and with constant transmit power to maximize average throughput [20]. Such a scheme consists of N signal constellations of size $M = 2^{n+1}$, where $n \in [1{:}\,N]$. In the process of M-QAM mode selection, the defined received SNR range is partitioned into N+1 non-overlapping regions. The boundaries of these regions are defined as the A-QASM switching level thresholds$\{\zeta_n\}_{n=1}^{N}$, with the extreme boundaries of the SNR range set as $\zeta_0 = 0$ and $\zeta_{N+1} = \infty$. An M-QAM mode n is chosen when the defined received SNR γ satisfies the following rule: $\zeta_n \leq \gamma < \zeta_{n+1}$. No transmission occurs when $\zeta_0 \leq \gamma < \zeta_1$to avoid deep fading. The adaptation occurs on a frame by frame basis as a means to maximize spectral efficiency in a slowly varying wireless fading channel. The design objective is to find the set of $\{\zeta_n | \, n = 1,2, \ldots, N\}$ switching thresholds that maximise average throughput while maintaining the target BER. We design an A-QASM scheme using N=5 signal constellations, namely 4, 8, 16, 32 and 64-QAM, which are modes 1, 2, 3, 4 and 5, respectively.

3 Statistics of Received SNR for Adaptive M-QAM Spatial Modulation

Let us consider conventional SM, in which, for each symbol period, a single active transmit antenna is selected from the set of all transmit antennae to transmit a symbol over the wireless fading channel $\boldsymbol{H}$. At the receive side, MRC is performed over L_r branches and an MRC SNR is thus associated with each possible active transmit antenna. For adaptive modulation schemes, the equivalent received SNR needs to be defined, as it is an important indicator of channel state and is directly used to adapt the data rate over the wireless channel in order to optimize spectral efficiency. Two approaches are proposed as definitions for the equivalent received SNR. The first approach defines the equivalent received SNR in terms of first order statistics, which entails selecting the lowest MRC SNR from a given transmit antenna activation and the second approach defines it in terms of average statistics. The latter is a heuristical approach which entails averaging the MRC SNR from all transmit antenna activations. The minimum SNR method is motivated by the fact that the average BER mainly depends on the largest instantaneous BER contribution which corresponds to the lowest MRC SNR.

3.1 First order statistics SNR

The received SNR, γ, for the first order statistic SNR approach in the A-QASM system is defined as

$$\gamma \triangleq \beta_1 \times min\{\gamma_1, \gamma_2, \dots, \gamma_{L_t}\}, \text{ where } \gamma_j \triangleq \sum_{i=1}^{L_r} \gamma_{ij} \text{ and j} \in [1: L_t]. \quad \text{(A.2)}$$

where γ_i is the MRC SNR for transmit antenna j. The scaling factor β_1 in (A.2) is included in order to take into account the instantaneous BER contributions from the other L_t-1 transmit antenna activations.

3.1.1 CDF and PDF of received SNR for A-QASM

Since (A.2) is the received SNR based on the minimum of the random Erlang distributed [15] SNR variables (r.v.), thus the law of order statistics [15] is used to derive the cumulative distribution function (CDF) and the probability density function (PDF) of the received SNR. It is necessary to perform these derivations in order to find the average BER analytical expressions for A-QASM schemes over a fading channel. The CDF and PDF for the first order statistics SNR in an $L_t \times L_r$ A-QASM scheme is given by (The detail derivation is shown in **Appendix A**):

$$F(\gamma) = 1 - \frac{\Gamma(\frac{\gamma}{\bar{\gamma}}, L_r)^{L_t}}{(L_r-1)!^{L_t}} \quad \text{(A.3)}$$

$$f(\gamma) = L_t \left(\frac{\Gamma(\frac{\gamma}{\overline{\gamma}} L_r)^{L_t - 1}}{(L_r - 1)!^{L_t - 1}} \right) \frac{\gamma^{L_r - 1}}{(L_r - 1)! \overline{\gamma}^{L_r}} e^{-\gamma / \overline{\gamma}} \quad \text{(A.4)}$$

where γ is defined in (A.2). $F(\gamma)$and $f(\gamma)$ are the CDF and PDF of the received SNR respectively and $\Gamma(x, a) \triangleq \int_x^\infty t^{a-1} e^{-t} dt$ is the upper incomplete Gamma function.

It is difficult to find a closed form average BER expression using (A.4), therefore, a PDF approximation strategy is employed. **NB:** The derivations in **Appendix A** exclude the scaling factor β_1 and it will only be included to scale the average SNR in the following subsection**.**

3.1.2 PDF Approximation using Maximum Likelihood Estimation

It is evident from (A.4) that the best PDF to fit to the distribution of the random SNR is the Gamma distribution [15]

$$f(\gamma) = \frac{\gamma^{\alpha - 1}}{\Gamma(\alpha) \theta^\alpha} e^{-\gamma / \theta} \quad \text{(A.5)}$$

The fitting of this distribution is carried out using a numerical method called maximum likelihood estimation [15]. In this section, the algorithm for determining the approximate PDF is stated and the approximated PDF for the different $L_t \times L_r$MIMO configuration is obtained.

Algorithm 1:

Step 1: Set $L_r \; and \; L_t$.

Step 2: Populate vector $\boldsymbol{Y}$ =$5n, n \in [1{:}\,19]$. This is the sample average linear SNR.

Step 3: Generate 1000 samples for random variable γ for each element of $\boldsymbol{Y}$**.**

- Solve *F*(γ)=*u* with respect to γ, where *u* is uniformly distributed in the interval [0,1) and *F*(γ) is defined in (A.3).
- Store all 1000 samples of γ in Vector $\boldsymbol{X}$**.**

Step 4: Fit $\boldsymbol{X}$ data to Gamma PDF using Gamma Fit function.

- $\boldsymbol{A} = GamFit(\boldsymbol{X})$ for each element of $\boldsymbol{Y}$**.**

Step 5: find the average of $\boldsymbol{A}$ using $\alpha = Mean(\boldsymbol{A})$.

Step 6: Fit $\boldsymbol{X}$ data to Gamma PDF with fixed parameter α (Step 5) using maximum likelihood estimation.

- Vector $\boldsymbol{B}$=$MLE(\boldsymbol{X}, GamPDF(\alpha))$, for each element of $\boldsymbol{Y}$.

Step 7: Find relation between Vector $\boldsymbol{B}$ and Vector $\boldsymbol{Y}$.

- θ=$PolyFit(\boldsymbol{Y}, \boldsymbol{B})$, fit to first order Polynomial.

NB:The functions *MLE*, *GamFit*, *GamPDF*, *Mean* and *Polyfit* are all inbuilt Matlab functions.

Algorithm 1 is used to find estimates for α and θ for the Gamma distribution given in (A.5).

Parameter θ varies with the average SNR defined in vector $\boldsymbol{Y}$ and Step 7 of the algorithm finds the linear relationship between the two variables. By applying the algorithm to find α and θ and using (A.5), an approximation for (A.4) is found. Parameter α is fixed to the value found in Step 5 of the algorithm.

3.1.3 PDF Approximation Results for an $L_t \times L_r$ A-QASM System

Based on the algorithm, the estimates of α and θ for the Gamma distribution can be found. For example, parameters α and θ of the Gamma distribution for 2×4 and 4×4 A-QASM systems are tabulated in Table A.1. Table A.1 also includes the scaling factor β_1 which only affects the average SNR for the A-QASM scheme. Hence, the scaling factor is used only to scale the average SNR.

Table A.1: Gamma PDF approximation parameters for an $\boldsymbol{L_t \times L_r}$ A-QASM System

$L_t \times L_r$	α	θ	β_1
2×4	5.0	$0.58\bar{\gamma}\beta_1$	1.20
4×4	6.2	$0.35\bar{\gamma}\beta_1$	1.32

NB: $\boldsymbol{\beta_1}$ is found graphically for each $\boldsymbol{L_t \times L_r}$ MIMO configuration by adjusting it manually until the theoretical BER graph matches the simulated BER graph.

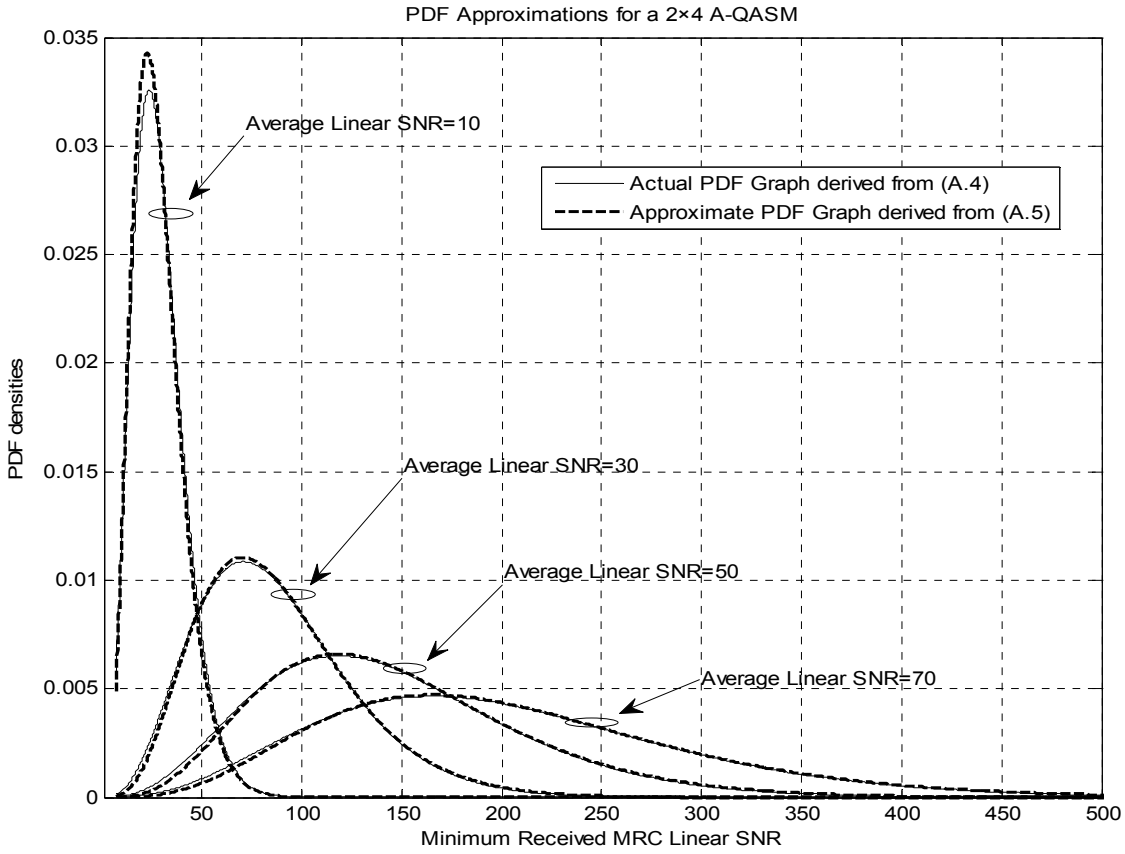

Fig. A.2 Comparison of the actual and the approximated PDF for a 2×4 A-QASM system

It is evident from Fig. A.2 that the PDF approximation in (A.5), without taking into consideration the scaling factor ($i.e\ \beta_1 = 1$), is a good estimate for the PDF defined in (A.4).

3.2 Average statistics SNR

In this approach, the average of the MRC SNR from all possible transmit antennae activations is taken into consideration. This is an alternative approach to the received SNR approach defined in (A.2). The equivalent received SNR for the average statistics SNR is defined as

$$\gamma \triangleq \frac{\beta_2}{L_t}\sum_{j=1}^{L_t}\sum_{i=1}^{L_r}\gamma_{ij}, \tag{A.6}$$

where γ_{ij} is the received SNR estimated at receive antenna i and from transmit antenna j. The scaling factor β_2 scales down the equivalent SNR. This is because the average MRC SNR

includes both the minimum and maximum received SNR. If the contribution of the maximum SNR is very high, the average MRC SNR will report a fairly good channel irrespective of the fact that some of the transmitter to receiver antenna channels might experience deep fading. Since the channel will be reported as good in this case, the A-QASM scheme will select a high data rate, which will induce a large number of bit errors in the deep faded channels and thus cause the target BER constraint to be violated. The scaling factor guards against this by scaling down the perceived channel state to as close as possible to the channel state that accurately describes the overall wireless channel over all possible wireless fading channels.

3.2.1 PDF of the Average SNR

The average statistics approach realizes a closed form expression for the average BER analytical expression. The PDF of the equivalent received SNR for the average statistics SNR is given by (The detailed derivation is shown in **Appendix B**).

$$f(\gamma) = \left(\frac{L_t}{\beta_2\,\overline{\gamma}}\right)^m \frac{\gamma^{m-1}}{(m-1)!} e^{-\gamma L_t / \beta_2\,\overline{\gamma}} \tag{A.7}$$

In the average statistics SNR approach, the scaling factor β_2 is set for each target BER. For example, Table A.2 shows the scaling factor of the 2×4 A-QASM and 4×4 A-QASM schemes at target BER=10^{-3}.

Table A.2: Scaling Factor $\boldsymbol{\beta_2}$ values for average statistics SNR

$L_t \times L_r$	β_2 Scaling Factor
2×4	0.71
4×4	0.54

N.B The scaling factor $\boldsymbol{\beta_2}$ is found graphically for each $\boldsymbol{L_t \times L_r}$ MIMO configuration with a specific target BER by manually adjusting it until the theoretical BER graph matches the simulated BER graph.

4 Adaptive Spatial Modulation Design

The aim of A-QASM is to optimize throughput over a MIMO wireless fading channel which is subject to an average target BER constraint. The design objective is to find the switching levels that optimize throughput but meet a target BER. In this Section we firstly derive the BER performance of A-QASM systems and then discuss the adaptive spatial modulation design.

4.1 BER Performance Analysis

In A-QASM, an M-QAM mode is selected based on channel state. There is a need to determine how different channel states are demarcated and this is done via the equivalent received SNR switching levels. The first step in determining the switching levels is the derivation of the average BER per A-QASM mode. Since we are comparing two received SNR approaches, the average BER per A-QASM mode needs to be determined for each approach. The average symbol error probability (SEP) for a given specific mode n, where $n \geq 1$, conditioned on the fading amplitude is given by:

$$P_k(error \cap mode\ n) = \int_{\zeta_n}^{\zeta_{n+1}} P(e|\gamma) \times f_k(\gamma) d\gamma\ ,\ k = 1,2 \qquad \text{(A.8)}$$

where $f_1(\gamma)$ and $f_2(\gamma)$ are the PDFs defined in (A.5) and (A.7) respectively and P_1 and P_2 are the average SEPs using the first order statistics SNR and the average statistics SNR, respectively; $P(e|\gamma)$ for M-QAM is given by [16]:

$$P(e|\gamma) = \frac{c}{d}\left(\frac{e^{-b\gamma/2}}{2} - c\frac{e^{-b\gamma}}{2} + (1-c)\sum_{i=1}^{d-1} e^{-b\gamma/S_i} + \sum_{i=n}^{2d-1} e^{-b\gamma/S_i}\right);$$

where $c = \left(1 - \frac{1}{\sqrt{M}}\right)$, $b = \left(\frac{3}{M-1}\right)$, $S_i = 2sin^2\theta_i$, $\theta_i = \frac{i\pi}{4d}$. d is the maximum number of summations.

Given $\int_{\zeta_n}^{\zeta_{n+1}} P(e|\gamma) \times f_k(\gamma) d\gamma = \int_{\zeta_n}^{\infty} P(e|\gamma) \times f_k(\gamma) d\gamma - \int_{\zeta_{n+1}}^{\infty} P(e|\gamma) \times f_k(\gamma) d\gamma$, the closed form solution of (A.8) is

$$P_k(error \cap mode\ n) = (A_k + B_k + C_k + D_k), \qquad k = 1,2 \qquad \text{(A.9)}$$

The conditional SEP based on (A.9) is

$$P_k(error \mid mode\ n) = (A_k + B_k + C_k + D_k)/\pi_n^k \qquad \text{(A.10)}$$

where π_n^1 and π_n^2 are defined as the probability of selecting mode *n* using the first order statistics and the average statistics SNR, respectively. π_n^k is given by

$$\pi_n^k \triangleq \int_{\zeta_n}^{\zeta_{n+1}} f_k(\gamma) d\gamma \tag{A.11}$$

After performing integration A_k , B_k, C_k, D_k and π_n^k are found and shown in Table A.3.

Table A.3: $\boldsymbol{A_k}$, $\boldsymbol{B_k, C_k, D_k}$ **and** $\boldsymbol{\pi_n^k}$ for first order statistics SNR and average statistics SNR

First order statistics SNR	Average statistics SNR
$A_1 = \frac{c}{2d\Gamma(\alpha)(\theta g)^\alpha}\{\Gamma(\zeta_n g, \alpha) - \Gamma(\zeta_{n+1} g, \alpha)\}$ $g = \frac{b\theta+2}{2\theta}$	$A_2 = \frac{c{L_t}^m}{2d\Gamma(m)(\beta_2\bar{\gamma} g)^m}\{\Gamma(\zeta_n g, m) - \Gamma(\zeta_{n+1} g, m)\}$ $g = \frac{b\beta_2\bar{\gamma}+2L_t}{2\beta_2\bar{\gamma}}$
$B_1 = \frac{-c^2}{2d\Gamma(\alpha)(\theta h)^\alpha}\{\Gamma(\zeta_n h, \alpha) - \Gamma(\zeta_{n+1} h, \alpha)\}$ $h = \frac{b\theta+1}{\theta}$	$B_2 = \frac{-c^2{L_t}^m}{2d\Gamma(m)(\beta_2\bar{\gamma} h)^m}\{\Gamma(\zeta_n h, m) - \Gamma(\zeta_{n+1} h, m)\}$ $h = \frac{b\beta_2\bar{\gamma}+L_t}{\beta_2\bar{\gamma}}$
$C_1 = \frac{c(1-c)}{d\Gamma(\alpha)\theta^\alpha}\sum_{i=1}^{d-1}\frac{1}{{w_i}^\alpha}\{\Gamma(\zeta_n w_i, \alpha) - \Gamma(\zeta_{n+1} w_i, \alpha)\}$ $w_i = \frac{b\theta+S_i}{\theta S_i}$	$C_2 = \frac{c(1-c){L_t}^m}{d\Gamma(m)(\beta_2\bar{\gamma})^m}\sum_{i=1}^{d-1}\frac{1}{{w_i}^m}\{\Gamma(\zeta_n w_i, m) - \Gamma(\zeta_{n+1} w_i, m)\}$ $w_{i=}\frac{b\beta_2\bar{\gamma}+S_i L_t}{\beta_2\bar{\gamma} S_i}$
$D_1 = \frac{c}{d\Gamma(\alpha)\theta^\alpha}\sum_{i=d}^{2d-1}\frac{1}{{w_i}^\alpha}\{\Gamma(\zeta_n w_i, \alpha) - \Gamma(\zeta_{n+1} w_i, \alpha)\}$	$D_2 = \frac{c{L_t}^m}{d\Gamma(m)(\beta_2\bar{\gamma})^m}\sum_{i=d}^{2d-1}\frac{1}{{w_i}^m}\{\Gamma(\zeta_n w_i, m) - \Gamma(\zeta_{n+1} w_i, m)\}$
$\pi_n^1 = \frac{\left\{\Gamma\left(\frac{\zeta_n}{\theta}, \alpha\right) - \Gamma\left(\frac{\zeta_{n+1}}{\theta}, \alpha\right)\right\}}{\Gamma(\alpha)}$	$\pi_n^2 = \frac{\left\{\Gamma\left(\frac{\zeta_n}{\beta_2\bar{\gamma}} L_t, m\right) - \Gamma\left(\frac{\zeta_{n+1}}{\beta_2\bar{\gamma}} L_t, m\right)\right\}}{\Gamma(m)}$

The parameters α and θ are found numerically using the maximum likelihood estimation, algorithm 1, described in Section 3. Since the objective of the A-QASM system is to optimize throughput for a given target BER, it is imperative to find the average conditional BER for M-QAM. It is assumed that there is only one possible bit error for each symbol error. This assumption holds for Gray coded M-QAM at high average SNR. Thus using (A.10), the average BER for M-QAM is given by [17]:

$$\overline{BER}_{nd}^k(\bar{\gamma}) \approx \frac{(A_k+B_k+C_k+D_k)}{\pi_n^k \times log_2 M}, \tag{A.12}$$

where *M* is the M-QAM constellation size.

In order to compare the average throughput of the proposed A-QASM with conventional SM, it is necessary to discuss conventional SM for a given target BER. For a given target BER the received SNR for conventional SM is partitioned into two regions, $0 \leq \gamma < \zeta_1$ for no transmission and $\zeta_1 \leq \gamma < \infty$ for transmission. The BER of conventional SM can be derived by setting $\zeta_n = \zeta_1$, and $\zeta_{n+1} = \zeta_2 = \infty$ into formulae in Table A.3.

Since the proposed adaptive modulation scheme is applied together with SM, there exists a transmit antenna estimation error probability. However, this error probability is independent of the A-QASM switching levels variation or design. Hence, the average transmit antenna estimation error probability remains the same as in [6, Eq.(19)].

$$\overline{BER}_{na}(\bar{\gamma}) \leq \sum_{j=1}^{L_t} \sum_{q=1}^{M} \sum_{\hat{\jmath}=1}^{L_t} \frac{N(j,\hat{\jmath}){\mu_\alpha}^{L_r}}{L_t M} \sum_{w=0}^{L_r-1} \binom{L_r+w-1}{w} [1-\mu_\alpha]^w, \tag{A.13}$$

where $\mu_\alpha = \frac{1}{2}\left(1 - \sqrt{\frac{{\alpha_\alpha}^2}{1+{\alpha_\alpha}^2}}\right)$ and ${\alpha_\alpha}^2 = \frac{\bar{\gamma}}{2}\left|x_q\right|^2$. $\bar{\gamma}$ is the average receive SNR per receive antenna, x_q is the q^{th} M-QAM symbol, $N(j,\hat{\jmath})$ is the number of bits in error between the transmit antenna index j and the estimated transmit antenna index $\hat{\jmath}$ and $\binom{L_r+w-1}{w}$ is the Binomial coefficient.

The upper bound, average BER in (A.13) for 4-QAM and 8-QAM SM is loose relative to the simulation and there exists a (~1 dB) difference between theory and simulation for both the 2×4 and 4×4 MIMO configurations. The bound is tightened by only taking into consideration the worst case scenario: for every transmit antenna index selected at the transmitter, the receiver estimates the transmit antenna index that has the highest Hamming distance relative to the actual transmit antenna index. This implies that the Hamming distance $N(j,\hat{\jmath})$ is always maximised for that particular number of transmit antennae L_t. Hence, for 4-QAM and 8-QAM, $N(j,\hat{\jmath}) = log_2(L_t)$, which is the limiting case.

The antenna estimation and symbol estimation processes are assumed independent as stated in [6]. The error probability (A.13) of the transmit antenna estimation is derived given that the symbol is perfectly detected. A similar assumption is made to derive the error probability of symbol detection. The error probability (Table A.3) of symbol estimation is derived given that

the transmit antenna index is perfectly detected. From these assumptions, the average BER per A-QASM mode n is lower bounded (best case) and is adapted from[6, Eq.(9)].

$$\overline{BER}_n^k(\bar{\gamma}) \geq \overline{BER}_{na}(\bar{\gamma}) + \overline{BER}_{nd}^k(\bar{\gamma}) - \overline{BER}_{na}(\bar{\gamma})\overline{BER}_{nd}^k(\bar{\gamma}), \tag{A.14}$$

In A-QASM, there exist two extremes when single modulation occurs. This is when the average received SNR is low and also when it is very high exceeding the avalanche SNR [18]. For the lowest average SNR, only the lowest signal constellation is selected as it is the only one that satisfies the target BER constraint. The other extreme case is when the average SNR exceeds the avalanche SNR and the A-QASM system only selects the highest signal constellation which maximizes the data throughput while meeting target BER constraint. The average BER for symbol estimation in (A.12) does not apply as the modulation has changed from A-QASM to conventional SM, hence the equation defined in [6, Eq.(12)] for conventional SM becomes relevant and it is applicable for both extreme cases. The equation that is applicable in these extreme cases is as shown,

$$\overline{BER}_d(\bar{\gamma}) \approx \frac{\frac{c}{d}\left\{\frac{1}{2}\left(\frac{2}{b\bar{\gamma}+2}\right)^{Lr} - \frac{c}{2}\left(\frac{1}{b\bar{\gamma}+1}\right)^{Lr} + (1-c)\sum_{i=1}^{d-1}\left(\frac{S_i}{b\bar{\gamma}+S_i}\right)^{Lr} + \sum_{i=d}^{2d-1}\left(\frac{S_i}{b\bar{\gamma}+S_i}\right)^{Lr}\right\}}{log_2(M)}, \tag{A.15}$$

where M=$\{4,64\}$ in this paper.

4.2 Adaptive Spatial Modulation design (Switching Levels)

To determine A-QASM switching levels for adaptive spatial modulation, the average BER of mode n in (A.14) is set to the target BER of P_0, thus $\overline{BER}_n^k(\bar{\gamma}) = P_0$. Since the closed form solutions for $\{\zeta_n | n = 1,2,\dots,N\}$ cannot be found, the alternative is to numerically search for these switching levels. The estimation of the switching level $\hat{\zeta}_n^k$ are thus found using the algorithm below from [19] with slight modification:

Step 1: Set $n = N$, and ζ_{N+1}=$+\infty$

Step 2: For each n, search for the unique $\zeta_n \epsilon [0, \zeta_{n+1})$ that satisfies

$$\hat{\zeta}_n^k = arg\min_{\zeta_n} \left(|\overline{BER}_n^k(\bar{\gamma}) - P_0|\right), \text{ where } |\cdot| \text{ is the absolute operator} \tag{A.16}$$

Step 3: If $n > 1$, Set $n = n - 1$, and go to Step 2. Otherwise, go to Step 4

Step 4: Set $\zeta_0 = 0$.

This method generates A-QASM switching level estimates for each average SNR value that maximizes average throughput. In this paper, $N = 5$ for A-QASM and $N = 1$ for conventional SM.

Then the overall average BER for the A-QASM system is given by [19]:

$$\overline{BER}^k(\bar{\gamma}) = \frac{\sum_{n=1}^{N} R_n \pi_n^k \overline{BER}_n^k(\bar{\gamma})}{\sum_{n=1}^{N} R_n \pi_n^k}, \quad \text{(A.17)}$$

where R_n is the number of bits per transmission for A-QASM mode n.

(A.17) provides a way of computing the average BER as the ratio of the average number of bits in error to the total average number of transmitted bits. (A.17) is the theoretical average BER for both the first order statistics SNR and the average statistics SNR which is used for comparison with the BER from simulations.

5 Simulation results

In this section, we use 2×4 and 4×4 A-QASM as examples to validate the analytical frameworks developed in Section 4 and provide BER and throughput performance comparisons between conventional SM and A-QASM. The average BER and average throughput are plotted against the average SNR at each receive antenna. The parameters regarding the AWGN and fading channel are consistent with those defined in Section 2. The following were assumed during simulation: Gray coded M-QAM constellation, frame size is 200 symbols, transmit and receive antennas are separated wide enough to avoid correlation and the total transmit power is the same for all transmissions [6].

5.1 Adaptive Spatial Modulation BER performance

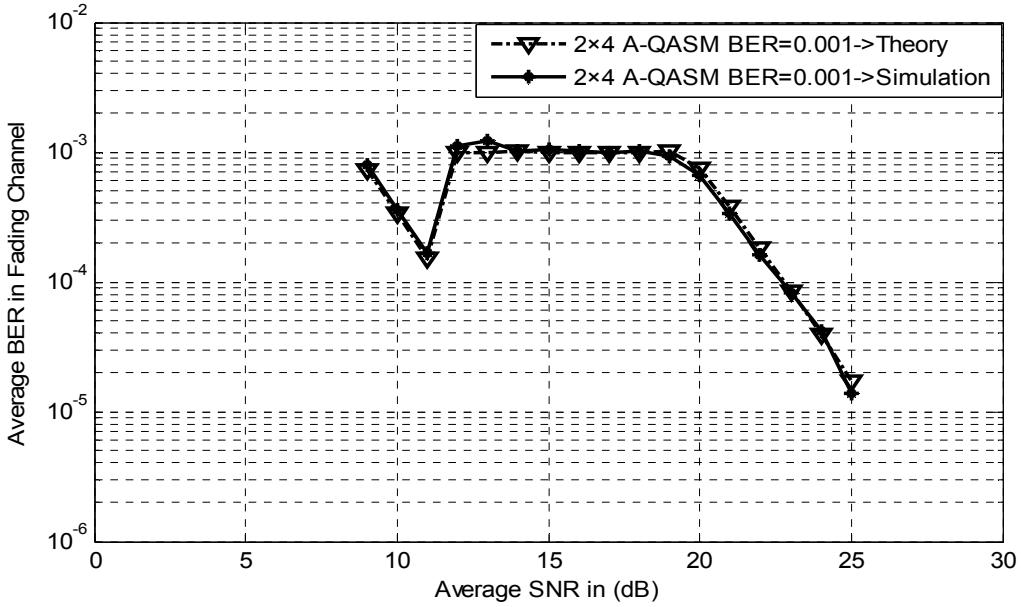

Fig. A.3 BER performance of $\mathbf{2 \times 4}$ A-QASM at $\boldsymbol{P_{target} = 10^{-3}}$ for first order statistics SNR

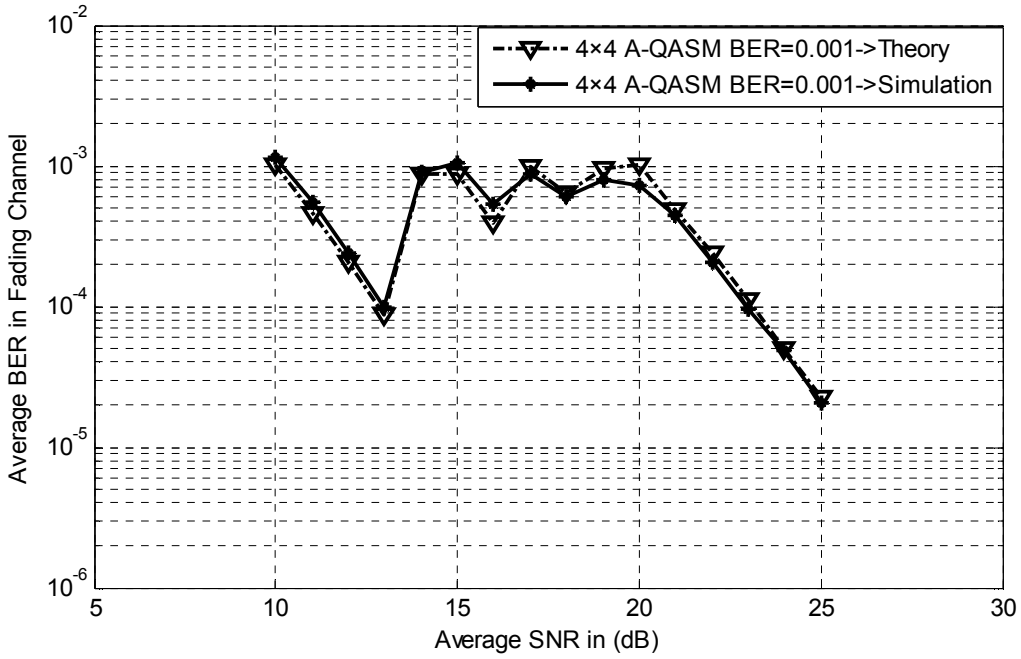

Fig. A.4 BER performance of $\mathbf{4 \times 4}$ A-QASM at $\boldsymbol{P_{target} = 10^{-3}}$ for first order statistics SNR

5.1.1 The first order statistics SNR

Fig. A.3 and Fig. A.4 show the comparison of the theoretical bounds and the average BER performance using the first order statistics SNR at $P_{target} = 10^{-3}$ for 2×4 and 4×4 A-QASM, respectively. As the results show in Fig. A.3 and A.4, theoretical bounds and simulation results match fairly well, validating the analytical expressions derived in Section 4 for the first order statistics SNR. The region from 9 dB to 11 dB in Fig. A.3 and 10 dB to 13 dB in Fig. A.4 are the regions when only the minimum modulation order (M=4 in our case) is the only modulation order that does not violate the BER constraint in that SNR range. Hence conventional SM takes place in that average SNR range, the same explanation is applicable for Fig. A.5 and A.6. The region from 12 dB to 19 dB in Fig. A.3 and the region from 14 dB to 20 dB in Fig. A.4 are the active regions for adaptive modulation. The 19 dB point in Fig. A.3 and 20 dB in Fig. A.4 are called the avalanche SNRs. At these avalanche points, there is a transition from adaptive modulation to conventional SM. The reason for this is that, the maximum data rate can be supported at average receive SNR values greater than the avalanche SNR whilst satisfying the average target BER in this case $P_{target} = 10^{-3}$. This is consistent with theory as shown in

Fig. A.3 and A.4. The average BER curve starts from 9 dB in Fig. A.3 and 10 dB in Fig. A.4 as opposed to 0 dB as in [18, Fig. 7(a)] because the average BER, with 4-QAM being the lowest selected M-QAM signal constellation below 9dB in Fig. A.3 and 10 dB in Fig. A.4, violates the $P_{target} = 10^{-3}$ BER constraint for average SNR below 9dB.

5.1.2 Average Statistics SNR

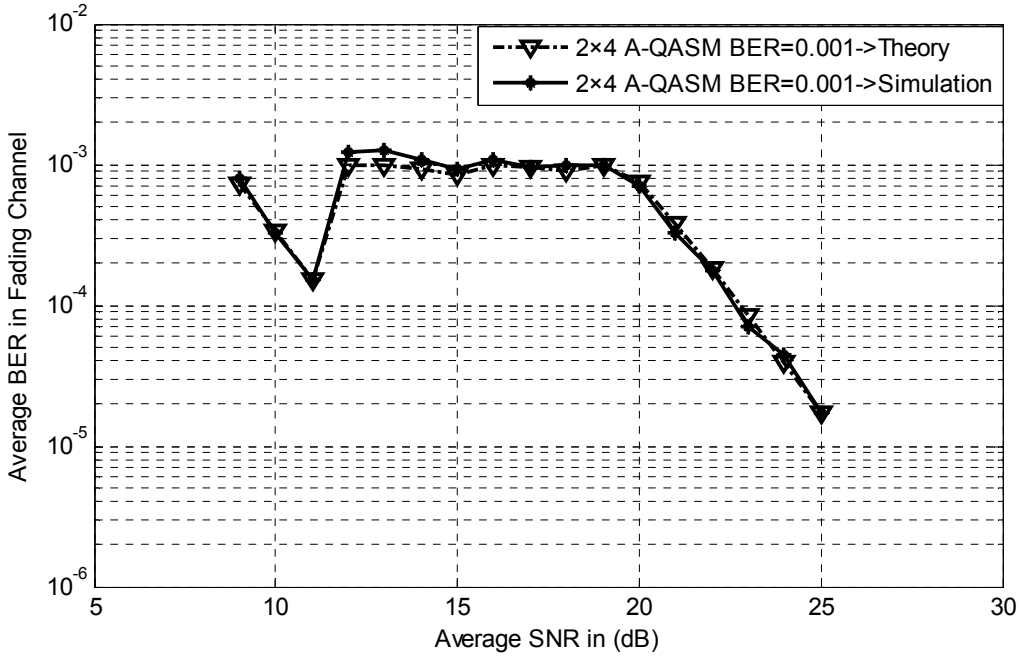

Fig. A.5 BER performance of $\mathbf{2 \times 4}$ A-QASM at $\boldsymbol{P_{target} = 10^{-3}}$ for average statistics SNR

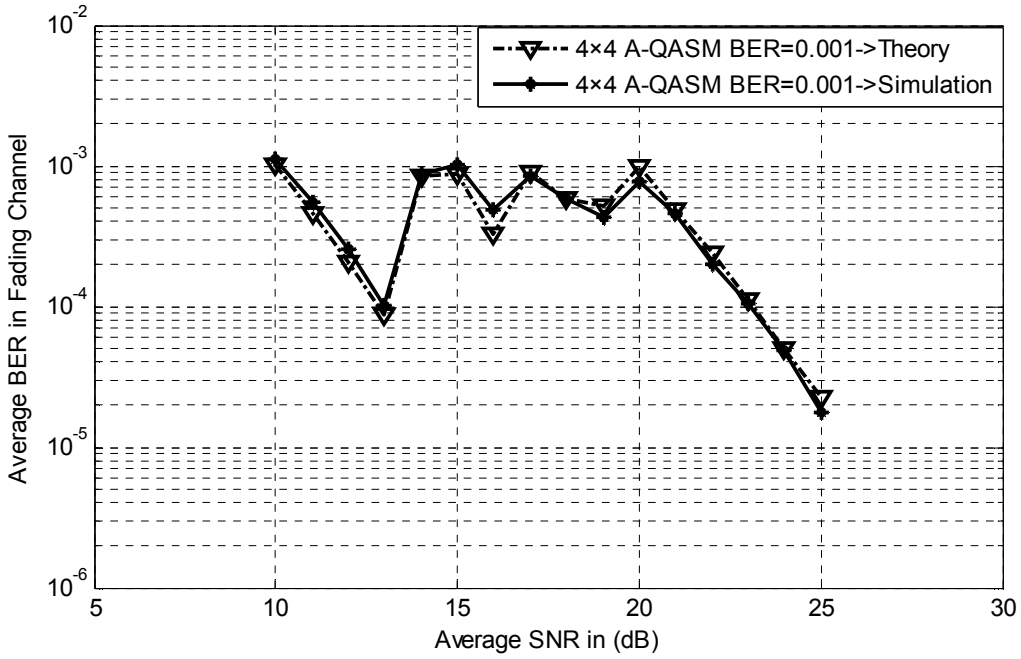

Fig. A.6 BER performance of $\mathbf{4 \times 4}$ A-QASM at $\boldsymbol{P_{target} = 10^{-3}}$ for average statistics SNR

Fig. A.5 and Fig. A.6 show the comparison of the theoretical bounds and the average BER performance using the average statistics SNR at $P_{target} = 10^{-3}$ for 2×4 and 4×4 A-QASM, respectively. Again, as the results show in Fig. A.5 and A.6, theoretical bounds and simulation results also match fairly well, validating the analytical expressions derived in Section 4 for the average statistics SNR. The adaptive SNR regions and avalanche points shown in Fig. A.5 and A.6 for 2×4 and 4×4 A-QASM are identical to those in Fig. A.3 and A.4. This demonstrates that the average statistics SNR is an alternative to the minimum statistics SNR. The 4×4 BER performance between 14 and 20 dB in Fig. A.4 and A.6 fluctuates between 10^{-3} and 4×10^{-4} as opposed to being constantly equal to the target BER as is the case with the 2×4 MIMO. This is as a result of a mixture of conventional SM for BER$< P_{target}$ and A-QASM for BER=P_{target}. Conventional SM is selected for a specific average SNR range as a result of the BER performance for other M-QAM modulation orders violating the target BER constraint. This forces the A-QASM to select only one modulation order, for a particular average SNR, which meets the target BER. This phenomenon is common in MIMO configurations with a high number of transmit antennae, as the BER performance for transmit antenna estimation is worse

because the probability of estimating an incorrect transmit antenna index increases with the number of transmit antennae.

5.2 Average throughput performance

The aim of this section is to compare average throughput between conventional SM and A-QASM. Both the average statistics SNR and the first order statistics SNR are simulated and average throughput curves at $P_{target} = 5 \times 10^{-5}$ are compared to validate the fact that both approaches can be used interchangeably to define equivalent received SNR.

5.2.1 The first order Statistics SNR

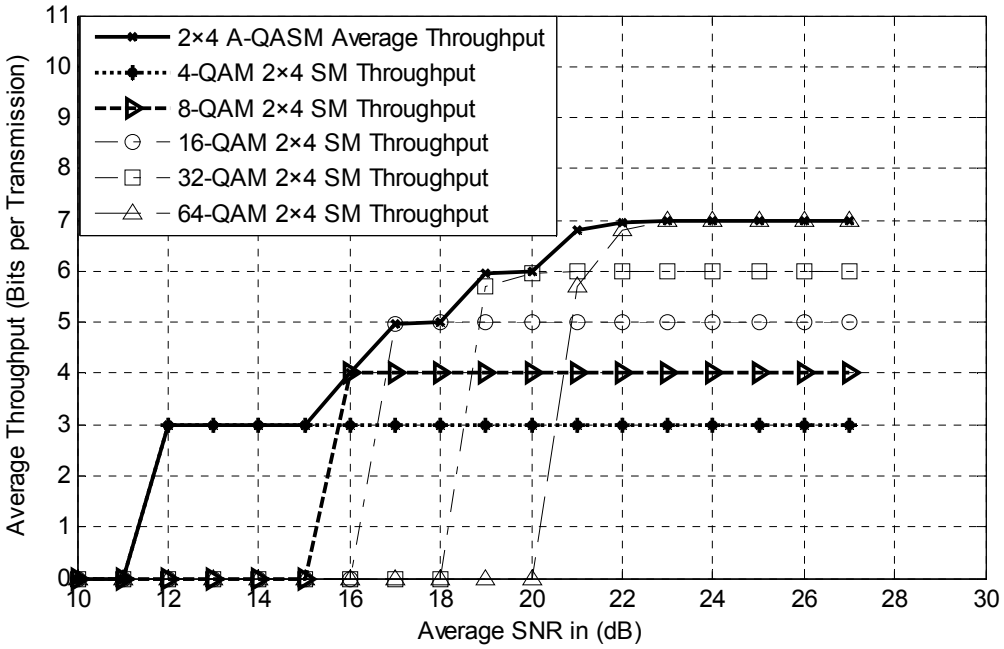

Fig. A.7 Throughput simulation of $\mathbf{2 \times 4}$ A-QASM scheme at $\boldsymbol{P_{target} = 5 \times 10^{-5}}$ for first order statistics SNR

Similar to the discussion in [18, Fig. 6(b)], Fig. A.7 shows the throughput simulation results of the conventional SM and 2×4 A-QASM system using the first order statistics SNR at $P_{target} = 5 \times 10^{-5}$. From the results shown in Fig. A.7, it is evident that the A-QASM scheme outperforms the conventional SM. The A-QASM scheme is temporarily equivalent in performance to the conventional SM scheme (4-QAM) at lower average SNR values because 4-

QAM is the only selected modulation at low average SNR values between 12 and 15 dB inclusive. From 15 dB to 22dB, the A-QASM system starts to outperform the conventional SM for all possible M-QAM levels (4, 8, 16, 32 and 64-QAM) because different signal constellations are being selected for a particular average SNR in order to maximize throughput. The conventional SM has no alternative but to transmit using the same data rate even if the channel permits for higher data rates to be sent via the wireless fading channel. At 23 dB and above, 64-QAM is the only modulation selected as the average SNR is high enough to ensure that the average target BER is met at this high data rate. At this point, the A-QASM scheme has the same throughput performance as the conventional SM. An interesting observation is that, for conventional SM (4, 8, 16, 32 or 64-QAM) transmission, the average throughput curves start from zero and gradually increase to the expected average throughput for that modulation (i.e $log_2(ML_t)$, where M is the M-QAM constellation size). Taking 64-QAM as an example, at 21 dB the average throughput is ~6 bits/symbol as opposed to the expected 7 Bits/symbol. This is a result of partial data transmission over the whole instantaneous SNR range. Data is not transmitted when the channel state is poor and this partitioning of the channel is determined by a SNR threshold limit that is found as described in Section 4 when $N = 1$. Data is thus transmitted only if the instantaneous received SNR exceeds this threshold. At 23 dB and above, the avalanche SNR is exceeded and the conventional SM transmission occurs for the full received SNR range.

5.2.2 Average Statistics SNR

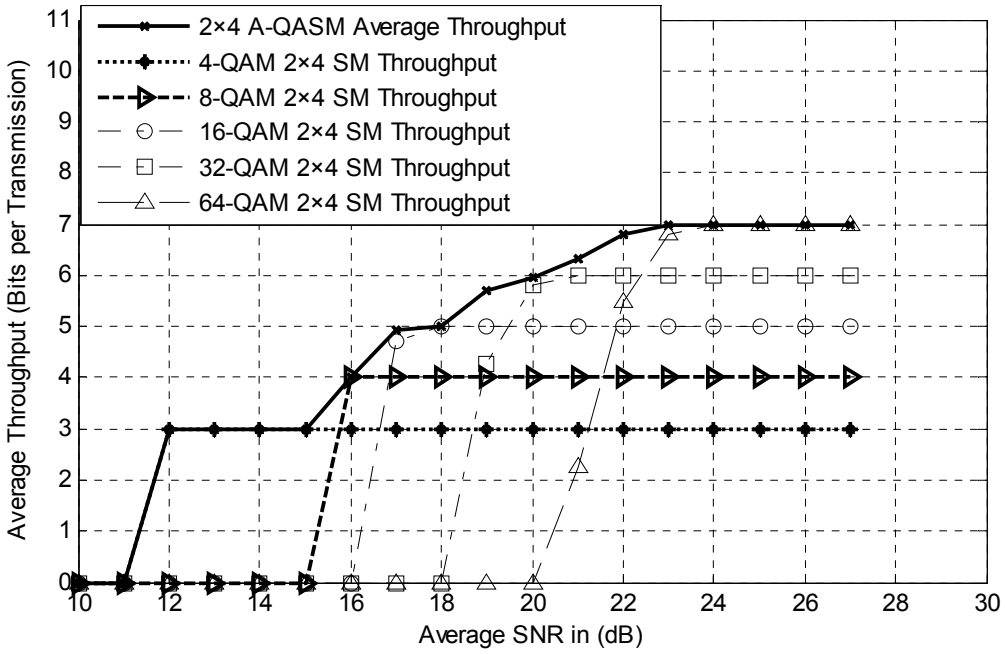

Fig. A.8 Throughput simulation of $\mathbf{2 \times 4}$ A-QASM scheme at $\boldsymbol{P_{target} = 5 \times 10^{-5}}$ for average statistics SNR

Fig. A.8 shows the average throughput for A-QASM scheme outperforms that of the conventional SM as expected. The only drawback is observed for the average throughput of the A-QASM scheme at 19 dB in Fig. A.7 and Fig. A.8. Since both these simulation results were obtained at $P_{target} = 5 \times 10^{-5}$, it is expected that their average throughput is the same. This is not the case as the average throughput at 19 dB in Fig. A.7 is 6 bits/symbol and that in Fig. A.8 is ~5.8 bits/symbol. This difference can be attributed to the fact that the switching level estimates in (A.16) are found using a numerical search method that attempts to minimize the difference between the BER of the system and the target BER. Therefore, in some cases, the closest possible BER to the target BER yields suboptimal average throughputs compared to BER that are equal to the target BER.

6 Conclusion

The adaptive M-QAM SM is investigated. The theoretical BER bound derived in Section 4 for A-QASM is successfully validated by the simulation results. It is also shown that the average throughput for the proposed A-QASM outperformed that of the conventional SM. The theoretical bounds and simulation results in Section 5 show that the two statistical SNR approaches, under the perfect channel state information assumption, can be used to define the equivalent received SNR interchangeably. However, the following facts need to be known:

First order statistics SNR:

- This approach has a complicated numerical approach for determining the average BER performance bound.
- This approach has the advantage over the average statistics SNR method that the scaling factor β_1 is set once for a specific MIMO configuration. The scaling factor is thus invariant with respect to average target BER unlike in the average SNR case.

Average statistics SNR:

- The advantage of this approach is that it has a closed form solution for the average theoretical BER performance bound.
- The disadvantage is that the scaling factor β_2 needs to be set as long as the average target BER is changed. Therefore, scaling factor β_2 is correlated to the average target BER.

Appendix

Appendix A
Derivation of the First Order Statistics CDF and PDF

The definition of a CDF is defined as [15]

$$F(c) = P(\gamma \leq c) = 1 - P(\gamma > c) \tag{A.18}$$

where γ is defined in (A.2) excluding the scaling factor β_1

From the definition of (A.2) we have

$$P(\gamma > c) = P((\gamma_1 > c) \cap (\gamma_2 > c) \cdots (\gamma_{L_t} > c)) \tag{A.19}$$

Since the received SNRs are i.i.d random variables, (A.19) can further be represented as

$$P(\gamma > c) = \prod_{j=1}^{L_t} P(\gamma_j > c) \tag{A.20}$$

where $\gamma_j, j \in [1: L_t]$, defined in (A.2) is a r.v. with Erlang distribution [15] which is given by

$$p(\gamma_j) = \frac{{\gamma_j}^{L_r-1}}{(L_r-1)!\bar{\gamma}^{L_r}} e^{-\gamma_j/\bar{\gamma}}, \tag{A.21}$$

and $\bar{\gamma}$ is the average received SNR per receive antenna and is identical for all γ_i .

Using (A.21) hence

$$P(\gamma_j > c) = \int_c^{\infty} p(\gamma_j) d\gamma_j = \frac{\Gamma(c/\bar{\gamma}, L_r)}{(L_r-1)!} \tag{A.22}$$

where $\Gamma(x, a) \triangleq \int_x^{\infty} t^{a-1} e^{-t} dt$ and is the upper incomplete Gamma function.

Since (A.22) is identical for all γ_j random variables, thus

$$P(\gamma > c) = \frac{\Gamma(c/\bar{\gamma}, L_r)^{L_t}}{(L_r-1)!^{L_t}} \tag{A.23}$$

Finally (A.18) becomes

$$F(\gamma) = 1 - \frac{\Gamma(\gamma/\overline{\gamma}, L_r)^{L_t}}{(L_r-1)!^{L_t}} \quad \text{(A.24)}$$

Based on $f(\gamma) = \frac{d}{d\gamma}(F(\gamma))$ the PDF of γ is given by

$$f(\gamma) = L_t \left(\frac{\Gamma(\frac{\gamma}{\overline{\gamma}}, L_r)^{L_t-1}}{(L_r-1)!^{L_t-1}} \right) \frac{\gamma^{L_r-1}}{(L_r-1)!\overline{\gamma}^{L_r}} e^{-\gamma/\overline{\gamma}}, \quad \text{(A.25)}$$

Appendix B
Derivation of Average Statistics PDF

Let the term $\gamma_j = \sum_{i=1}^{L_r} \gamma_{ij}$, the expression of (A.6) is simplified to

$$\gamma = \sum_{j=1}^{L_t} \frac{\beta_2}{L_t} \gamma_j, \text{ where } j \in [1: L_t] \quad \text{(A.26)}$$

Now Taking the MGF [15] of the r.v., $\frac{\beta_2}{L_t}\gamma_j$, which is distributed according to the Erlang distribution defined in (A.21) $p(\gamma_j)$, we get

$E_{\gamma_j}\left(e^{\frac{s\beta_2\gamma_j}{L_t}}\right) = \int_0^\infty p(\gamma_j)\, e^{\frac{s\beta_2\gamma_j}{L_t}} d\gamma_j$, where $E(\cdot)$ the expectation operator and s is is the Laplace variable.

The closed form MGF solution for the integral above is

$$E_{\gamma_j}\left(e^{\frac{s\beta_2\gamma_j}{L_t}}\right) = \left(\frac{\beta_2\overline{\gamma}}{L_t}\right)^{-L_r} \left(\frac{1}{\frac{\beta_2\overline{\gamma}}{L_t}} - s\right)^{-L_r} \quad \text{(A.27)}$$

Since the $\frac{\beta_2}{L_t}\gamma_j$ is i.i.d the MGF of the received average SNR defined in (A.6) is a product of the MGF in (A.27). The expression in (A.6) is equivalent to the sum of the independent random variables $\frac{\beta_2}{L_t}\gamma_j$ [15] which imply to

$$E_\gamma(e^{s\gamma}) = \left(\frac{\beta_2\overline{\gamma}}{L_t}\right)^{-L_rL_t} \left(\frac{1}{\frac{\beta_2\overline{\gamma}}{L_t}} - s\right)^{-L_rL_t} \quad \text{(A.28)}$$

Defining m≜ L_tL_r, thus (A.28) simplifies to

$E_\gamma(e^{s\gamma}) = \left(\frac{\beta_2\overline{\gamma}}{L_t}\right)^{-m}\left(\frac{1}{\frac{\beta_2\overline{\gamma}}{L_t}} - s\right)^{-m}$, to find the PDF from the MGF, an inverse Laplace Transform is carried out and the PDF is given below from the inverse Laplace Transform Tables in [21]

$$f(\gamma) = \left(\frac{L_t}{\beta_2\overline{\gamma}}\right)^m \frac{\gamma^{m-1}}{(m-1)!} e^{-\gamma L_t/\beta_2\overline{\gamma}} \quad \text{(A.29)}$$

References

[1] R.Y. Mesleh, H. Haas, C. W. Ahn, S. Yun, "Spatial modulation-a new low complexity spectral efficiency enhancing technique", in *Proc. ChinaCOM, Beijing,* pp. 1-5, 2006.

[2] R.Y Mesleh, H. Haas, S. Sinanovic, C. W. Ahn, S. Yun, "Spatial modulation", *IEEE Transactions on vehicular technology*, vol. 57, no.4, pp. 2228-2241, Jul. 2008.

[3] P. Wolniansky, G. Foschini, G. Golden and R. Valenzuela, "V-BLAST: An Architecture for Realizing very High Data Rates over the Rich- Scattering Wireless Channel", in *Proc URSI Int. Symp. on Signals ,Systems and Electronics (ISSSE '98.)*, Pisa, pp. 295–300, 1998.

[4] M. D. Renzo, H. Haas, and P. M. Grant, "Spatial Modulation for Multiple-Antenna Wireless System: A Survey", *IEEE Communications Magazine, pp.182-191, Dec. 2011*

[5] J. Jeganathan, A. Ghrayeb, and L. Szczecinski, "Spatial Modulation: Optimal Detection and Performance Analysis", *IEEE Commun. Lett.,*vol. 12, no. 8, pp. 545-547, 2008.

[6] N. R. Naidoo, H. Xu and T. Quazi, "Spatial Modulation: Optimal Detector Asymptotic Performance and Multiple-stage Detection", *IET proceedings Communications,* Vol. 5, no. 10, pp. 1368-1376, 2011**.**

[7] H. Xu, "Simplified ML Based Detection Schemes for M-QAM Spatial Modulation Trellis coded spatial modulation", *IET proceedings Communications*, Vol. 6, Issue 11, pp. 1356-1363, 2012.

[8] J. Wang, S. Jia and J. Song, "Signal Vector Based Detection Scheme for Spatial Modulation", *IEEE Commun. Lett.,*vol. 16, no. 1, pp. 19-21, 2012.

[9] R. Mesleh, M. D. Renzo, H. Haas, and P. M. Grant, "Trellis coded spatial modulation", *IEEE Trans. on wireless Comms.*, vol. 9, no. 7, pp. 2349-2361, July 2010.

[10] S. Hwang, S. Jeon, S. Lee and J. Seo, "Soft-output ML detector for OFDM spatial modulation systems", *IEICE Electronics Express*, vol. 6, no.19, pp. 1426-1431, 2009.

[11] E. Basar, U. Aygolu, E. Panayırcı and H. V. Poor, "New Trellis Code Design for Spatial Modulation", *IEEE Trans. on wireless Comms.*, vol. 10, no. 8, pp. 2670-2680, August 2011.

[12] J. Jeganathan, A. Ghrayeb, and L. Szczecinski, "Space Shift Keying Modulation for MIMO Channels", *IEEE Trans. on Wireless Comms.*, vol. 8, no. 7, pp. 3692-3703, 2009.

[13] P. Yang, Y. Xiao, Y. Yu and S. Li, "Adaptive Spatial Modulation for Wireless MIMO Transmission Systems", *IEEE Commun. Lett.,*vol. 15, no. 6, pp. 602-604, 2011.

[14] J. Ham, M. S. Kim, C. Lee, and T. Hwang, “An adaptive modulation algorithm for performance improvement of MIMO ML systems”, *IEEE Commun. Lett.*, vol. 12, no. 11, pp. 819-821, 2008.

[15] C.W. Helstrom, “Probability and Stochastic Processes for Engineers”, *Macmillan Publishing Company*, 1984.

[16] H. Xu, “Symbol error probability for generalized selection combining reception of M-QAM”, *SAIEE Africa Research Journal, Vol. 100, No. 3, pp.68-71, 2009*

[17] J.G. Proakis, “Digital communications*”, McGraw-Hill, New York*, 2001, 4th edn.

[18] B. Choi, L. Hanzo, “Optimum Mode-Switching-Assisted Constant-power Single-and Multicarrier Adaptive Modulation”, *IEEE Transactions on Vehicular Technology*, Vol.52, No.3,pp.536-560, May 2003.

[19] Q. Liu, S. Zhou, G.B Giannakis “Queing with Adaptive Modulation and Coding over Wireless Links: Cross Layer Analysis and Design”, *IEEE Transactions on wireless communications*, Vol.4,No.3 , pp.1142-1153, May 2005.

[20] M. S. Alouini and A. J. Goldsmith, “Adaptive modulation over Nakagami fading channels” , *J. Wireless Commun.*, vol. 13, no. 1–2, pp.119–143, 2000.

[21] K. Ogata, "Modern Control Engineering", *Prentice Hall; 3 Sub edition*, 1996.

Paper B

Spatial Modulation over *K* Multiplicative Complex Fading Wireless Channels

B.M. Mthethwa and H. Xu

Fully Accepted for Publication at IET Communications Journal

Abstract

We apply spatial modulation (SM) over multiplicative complex fading wireless channels, where the multiplicative complex fading is represented by the product of *K* statistically independent and identically distributed (i.i.d) standard complex Gaussian random variables, where $K \geq 2$. The analytical bit error rate (BER) approximation of symbol estimation is obtained in terms of a Meijer's G function. The conditional pairwise error probability (PEP) of transmit antenna index estimation is a function of a stochastic parameter with an unknown distribution function. We propose a lognormal distribution to approximate the distribution of this stochastic parameter. Based on the lognormal distribution, the average PEP and the analytical error probability upper bound of transmit antenna index estimation are derived. A goodness of fit test successfully validates the proposed lognormal distribution being the approximate distribution of the stochastic parameter. The derived analytical BER approximations for both symbol and transmit antenna index estimation are successfully validated via Monte-Carlo simulations.

1 Introduction

SM is a multiple-input-multiple-output (MIMO) scheme proposed by Mesleh et al, [1] that eliminates transmit antenna synchronization and inter-channel interference, thus reducing receiver complexity compared to MIMO V-BLAST (Vertical-Bell Laboratories Layered Space-Time architecture) transmission [2]. SM has been studied extensively over i.i.d and correlated Rayleigh fading channels for example in [1] and [3]. Of late, research attention has been broadened to other wireless fading channel models. For example, the Weibull fading channel model fits the short-term experimental fading channels for mobile communications well and the lognormal wireless fading channel model provides a good fit to the long-term fading environment as discussed in [4] and [5], respectively. The other wireless fading channel model of interest is the multiplicative fading channel, where the fading process observed at the single receive antenna is represented by the product of K statistically independent fading processes. This model closely matches measurements made in a forest [6] or city centre environment, where there is a very high probability of diffraction. As a consequence of multiple cascaded fading channels, the probability of deep fading is greater than that of conventional single fading (K=1) environments.

Tran et al [7] applies signal space diversity over a generalized K-Nakagami-m multiplicative fading channel and suggests an approach for mitigating the fading severity by increasing the diversity constellation. As a result of growing interest in this wireless fading channel model, [8] and [9] derive useful statistical distributions for a multiplicative fading channel. However, to the authors' best knowledge none of the literature research work has developed an analytical framework for SM over multiplicative fading channels. This is particularly useful as it provides a benchmark for research work carried out with the objective to improve the error probability of SM in a city centre or forest like environment. We therefore take the opportunity to derive the analytical BER approximations for both symbol and antenna index estimation and also propose an accurate approximation method for determining the conditional PEP of SM for this type of fading channel.

The rest of the paper is organized as follows: Section 2 describes the system model for SM over multiplicative complex fading channels. In Section 3, an analytical approach for the derivation of the asymptotic error probability performance of SM over multiplicative fading channels is

discussed. In Section 4, Monte-Carlo simulations validate the analytical expressions derived in Section 3. Section 5 concludes the paper.

2 System Model

We consider an $L_t \times L_r$ M-ary quadrature amplitude modulation (MQAM) SM system model as discussed in [1], where L_t and L_r are the number of transmit and receive antenna in the MIMO configuration, respectively. The SM transmission is done over an $L_r \times L_t$ wireless fading channel matrix $\boldsymbol{H}$ with each entry being a product of K i.i.d standard complex Gaussian random variables. Each entry of the channel matrix $\boldsymbol{H}$ is represented mathematically by

$$h_{ij} \triangleq \prod_{p=1}^{K} \alpha_{ijp}, \tag{B.1}$$

where$p \in [1:K]$, $i \in [1:L_r]$, $j \in [1:L_t]$, $\alpha_{ijp} \sim CN(0,1)$and h_{ij} is the complex fading coefficient for the j^{th} transmit antenna to the i^{th} receive antenna wireless path. The random variable α_{ijp} is the p^{th} complex fading coefficient of the j^{th} transmit antenna to the i^{th} receive antenna wireless path. The channel matrix $\boldsymbol{H}$ entries change from block to block and hence the channel is block fading, with 1 block being defined as carrying N_b bits. The received signal vector at the receiver is given by [3]

$$\boldsymbol{y} = \sqrt{\bar{\gamma}}\boldsymbol{H}\boldsymbol{x}_{jq} + \boldsymbol{n}, \tag{B.2}$$

where $\boldsymbol{y} = \left[y_1\ y_2\ \cdots y_{L_r}\right]^T$ represents the received signal vector, $\bar{\gamma}$ is the average received signal-to-noise ratio (SNR) at each receive antenna, $\boldsymbol{x}_{jq}$ is the transmitted signal vector of the q^{th} MQAM symbol from transmit antenna j, where $q \in [1:M]$ and $[\cdot]^T$ is the transpose operation. $\boldsymbol{n} = \left[n_1\ n_2\ \cdots n_{L_r}\right]^{\boldsymbol{T}}$ is the additive white Gaussian noise (AWGN) vector with i.i.d entries according to the standard complex Gaussian distribution $CN(0,1)$.

It is assumed that full channel knowledge is available at the receiver and the wireless channels are frequency flat. At the receiver, a maximum ratio combiner is used for optimal performance together with SM optimal detection [20] for joint estimation of the transmitted MQAM symbol and transmit antenna index.

3 Asymptotic error probability analysis of SM

In this section, we derive the asymptotic error probability of SM over multiplicative complex fading channels. The SM detector is responsible for the estimation of two quantities: the active transmit antenna index and transmitted symbol. The antenna index estimation and transmitted symbol estimation are assumed independent as stated in [3]. The error probability of the transmit antenna estimation is derived given that the transmitted MQAM symbol is perfectly detected. A similar assumption is made to derive the error probability of MQAM symbol detection. The error probability of transmitted MQAM symbol estimation is derived given that the transmit antenna index is perfectly detected. From these assumptions, we deduce that the BER is lower bounded (best case) for SM and is given by [3, Eq.(9)]

$$\overline{BER}(\bar{\gamma}) \geq \overline{BER}_a(\bar{\gamma}) + \overline{BER}_d(\bar{\gamma}) - \overline{BER}_a(\bar{\gamma})\overline{BER}_d(\bar{\gamma}), \tag{B.3}$$

where $\overline{BER}_a(\bar{\gamma})$ is the bit error rate of transmit antenna index estimation and $\overline{BER}_d(\bar{\gamma})$ is the bit error rate of transmitted symbol estimation.

3.1 Analytical BER approximation of transmitted symbol estimation

Assuming perfect transmit antenna index detection, the SM detector applies the maximum likelihood criteria to estimate the most likely transmitted symbol as follows [3, Eq.(10)]

$$x_{\hat{q}} = arg\min_{q} \sqrt{\bar{\gamma}}\left\|\boldsymbol{g}_{jq}\right\|_F^2 - 2Re\{\boldsymbol{y}^H\boldsymbol{g}_{jq}\}, \tag{B.4}$$

where $x_{\hat{q}}$ is the estimated symbol $\boldsymbol{g}_{jq} = \boldsymbol{h}_j x_q$, $\boldsymbol{h}_j$ denotes the j^{th} column of the channel matrix $\boldsymbol{H}$, x_q is the q^{th} symbol from the MQAM signal constellation and $(\cdot)^H$ is the Hermitian operator. The error probability derivation of the transmitted symbol estimation requires the probability density function (PDF) of the received SNR over a multiplicative fading channel at each receive antenna to be known.

3.1.1 PDF of the received SNR

Since the complex fading at a receive antenna is modeled by (B.1), it follows that the fading gain at a receive antenna is the product of *K* i.i.d Rayleigh distributed fading gains. In [8], the PDF of the received SNR over a wireless channel with *K* cascaded independent Nakagami-m fading gains is derived and shown to be [8, Eq.(14)]

$$f(\gamma_i) = \frac{1}{\gamma_i \prod_{p=1}^{K} \Gamma(m_p)} G_{0\ K}^{K\ 0}\left(\frac{\gamma_i}{\bar{\gamma}_i} \prod_{p=1}^{K} m_p \,\middle|\, \begin{matrix} - \\ m_1,\ldots,m_K \end{matrix}\right), \tag{B.5}$$

where $\Gamma(a) \triangleq \int_0^\infty t^{a-1}e^{-t}dt$ is the gamma function and $G_{p\ q}^{m\ n}\left(z\middle|\begin{matrix} a_1,\ldots,a_p \\ b_1,\ldots,b_q \end{matrix}\right)$ is the Meijer's G function that is defined and explained in [9, Eq.(4)].

Based on (B.5), the PDF of the received SNR in our study is found by setting the fading intensity (m_p) to unity since the individual fading gains are Rayleigh distributed. Thus the following simplifications to (B.5) can be done:

$\prod_{p=1}^{K} \Gamma(m_p) = 1$ and $\prod_{p=1}^{K} \mathrm{m}_p = 1$. Hence (B.5) becomes

$$f(\gamma_i) = \frac{1}{\gamma_i} G_{0\ K}^{K\ 0}\left(\frac{\gamma_i}{\bar{\gamma}} \,\middle|\, \begin{matrix} - \\ 1,\ldots,1 \end{matrix}\right), \tag{B.6}$$

The received SNR γ_i are i.i.d hence, $\bar{\gamma}_i = \bar{\gamma}$, for $i \in [1{:}\, L_r]$. For the rest of the paper, the PDF of the received SNR for each receive antenna is defined by (B.6).

3.1.2 Moment Generating Function approach of deriving average bit error probability

The moment generating function (MGF) for the received SNR at receive antenna *i* is given by

$$M(\gamma_i) \triangleq E(e^{-s\gamma_i}) = \int_0^\infty \frac{1}{\gamma_i} G_{0\ K}^{K\ 0}\left(\frac{\gamma_i}{\bar{\gamma}} \,\middle|\, \begin{matrix} - \\ 1,\ldots,1 \end{matrix}\right) e^{-s\gamma_i} d\gamma_i, \tag{B.7}$$

where $E(\cdot)$ is the expectation operator, and *s* is the Laplace operator.

Using Eq.(7.813/1) in [10] (B.7) simplifies to

$$M(\gamma_i) = G_{1\ K}^{K\ 1}\left(\frac{1}{\bar{\gamma} \cdot s} \,\middle|\, \begin{matrix} 1 \\ 1,\ldots,1 \end{matrix}\right), \tag{B.8}$$

Since we are dealing with fading over a spatially diverse MIMO scheme, it becomes imperative to determine the average BER due to fading over L_r receive branches. In SM, a maximal ratio combiner (MRC) is used to combine signals from L_r receive branches before SM detection is employed to estimate both transmit antenna index and modulated symbol. Based on MRC, the total received SNR is given by

$$\gamma \triangleq \sum_{i=1}^{L_r} \gamma_i, \tag{B.9}$$

Since $\gamma_i, \forall\, i \in [1: L_r]$ are i.i.d, hence the MGF of the total received SNR γ is given by

$$M(\gamma) = \prod_{i=1}^{L_r} G_{1\ K}^{K\ 1}\left(\frac{1}{\bar{\gamma}_S}\middle|\begin{matrix}1\\1,\ldots,1\end{matrix}\right), \tag{B.10}$$

Using Eq.(9.21) in [12], we get the symbol error rate of MQAM modulation:

$$\overline{SER}_d(\bar{\gamma}) \triangleq \frac{4}{\pi}\left(1-\frac{1}{\sqrt{M}}\right)\int_0^{\frac{\pi}{2}} M(\gamma)d\vartheta - \frac{4}{\pi}\left(1-\frac{1}{\sqrt{M}}\right)^2 \int_0^{\frac{\pi}{4}} M(\gamma)d\vartheta, \tag{B.11}$$

where s in (B.10) is now defined as $s=\frac{g_{QAM}}{\sin^2\vartheta}$ and $g_{QAM} = \frac{3}{2(M-1)}$ based on [12] and M is the QAM signal constellation size.

By defining $a \triangleq \left(1-\frac{1}{\sqrt{M}}\right)$ and substituting (B.10) into (B.11) we obtain

$$\overline{SER}_d(\bar{\gamma}) = \left\{\frac{4}{\pi}a\int_0^{\pi/2}\prod_{i=1}^{L_r} G_{1\ K}^{K\ 1}\left(\frac{\sin^2\vartheta}{\bar{\gamma}g_{QAM}}\middle|\begin{matrix}1\\1,\ldots,1\end{matrix}\right)d\vartheta - \frac{4}{\pi}a^2\int_0^{\pi/4}\prod_{i=1}^{L_r} G_{1\ K}^{K\ 1}\left(\frac{\sin^2\varphi}{\bar{\gamma}g_{QAM}}\middle|\begin{matrix}1\\1,\ldots,1\end{matrix}\right)d\varphi\right\}, \tag{B.12}$$

In (B.12) the integration variables are changed for convenience. We are now integrating with respect to ϑ and φ. Applying the trapezoidal numerical integration rule [13] to evaluate the integrals, we further get the following approximations for the two integrals:

Integral (i): $\Delta_1 \triangleq \int_0^{\pi/2}\prod_{i=1}^{L_r} G_{1\ K}^{K\ 1}\left(\frac{\sin^2\vartheta}{\bar{\gamma}g_{QAM}}\middle|\begin{matrix}1\\1,\ldots,1\end{matrix}\right)d\vartheta$,

$$\Delta_1 \approx \frac{\pi}{4n}\left\{\prod_{i=1}^{L_r} G_{1\ K}^{K\ 1}\left(\frac{\sin^2\left(\frac{\pi}{2}\right)}{\bar{\gamma}g_{QAM}}\middle|\begin{matrix}1\\1,\ldots,1\end{matrix}\right) + 2\sum_{k=1}^{n-1}\prod_{i=1}^{L_r} G_{1\ K}^{K\ 1}\left(\frac{\sin^2\vartheta_k}{\bar{\gamma}g_{QAM}}\middle|\begin{matrix}1\\1,\ldots,1\end{matrix}\right)\right\}, \tag{B.13}$$

where $\vartheta_k = \frac{k\pi}{2n}$.

Integral (ii): $\Delta_2 \triangleq \int_0^{\pi/4}\prod_{i=1}^{L_r} G_{1\ K}^{K\ 1}\left(\frac{\sin^2\varphi}{\bar{\gamma}g_{QAM}}\middle|\begin{matrix}1\\1,\ldots,1\end{matrix}\right)d\varphi$,

$$\Delta_2 \approx \frac{\pi}{8n}\left\{\prod_{i=1}^{L_r} G_{1\ K}^{K\ 1}\left(\frac{\sin^2\left(\frac{\pi}{4}\right)}{\bar{\gamma}g_{QAM}}\middle|\begin{matrix}1\\1,\ldots,1\end{matrix}\right) + 2\sum_{k=1}^{n-1}\prod_{i=1}^{L_r} G_{1\ K}^{K\ 1}\left(\frac{\sin^2\varphi_k}{\bar{\gamma}g_{QAM}}\middle|\begin{matrix}1\\1,\ldots,1\end{matrix}\right)\right\}, \tag{B.14}$$

where $\varphi_k = \frac{k\pi}{4n}$.

In (B.13) and (B.14), n is the maximum number of summations. In our case n=20.

Assuming that only one bit error occurs per symbol error at high average SNR and when using gray-coded mapping we can approximate the BER as follows: [14]

$\overline{BER}_d(\bar{\gamma}) \approx \overline{SER}_d(\bar{\gamma}) / \log_2 M$,

$$\overline{BER}_d(\bar{\gamma}) \approx \frac{4a(\Delta_1 - a\Delta_2)}{\pi \log_2 M}, \quad \text{(B.15)}$$

where $\Delta_1$and Δ_2 are given in (B.13) and (B.14), respectively.

3.2 Analytical BER of transmit antenna index estimation

The average BER for transmit antenna index estimation, given that the symbol estimation process is perfect, is union bounded by [14, pp. 261-262]

$$\overline{BER}_a(\bar{\gamma}) \leq E_j\left[\sum_{\hat{\jmath}} N(j,\hat{\jmath})\, P\left(x_{jq} \rightarrow x_{\hat{\jmath}q}\right)\right], \quad \text{(B.16)}$$

where $E_j(\cdot)$ is the statistical expectation function. The expression in (B.16) is equivalent to the following: [3, Eq.(13)]

$$\overline{BER}_a(\bar{\gamma}) \leq \frac{\sum_{j=1}^{L_t} \sum_{q=1}^{M} \sum_{\hat{\jmath}=1}^{L_t} N(j,\hat{\jmath}) P\left(\boldsymbol{x}_{jq} \rightarrow \boldsymbol{x}_{\hat{\jmath}q}\right)}{L_t M}, \quad \text{(B.17)}$$

where $P\left(\boldsymbol{x}_{jq} \rightarrow \boldsymbol{x}_{\hat{\jmath}q}\right)$ is the pairwise error probability of choosing signal vector $\boldsymbol{x}_{\hat{\jmath}q}$given that $\boldsymbol{x}_{jq}$ was transmitted. $N(j,\hat{\jmath})$ is the number of bits in error between transmit antenna index j and estimated transmit antenna index $\hat{\jmath}$.

The PEP conditioned on channel matrix $\boldsymbol{H}$ is derived as in [3, Eq.(14)] and is given by

$$P\left(\boldsymbol{x}_{jq} \rightarrow \boldsymbol{x}_{\hat{\jmath}q} | \boldsymbol{H}\right) = Q\left(\sqrt{v}\right), \quad \text{(B.18)}$$

where $Q(x) = \frac{1}{\pi}\int_0^{\pi/2} e^{-x^2/2\sin^2\theta} d\theta$ and random parameter v is defined in [15, Eq.(5)] as

$$v \triangleq \frac{\overline{\gamma}}{2}\left|x_q\right|^2 \left\|\boldsymbol{h}_j - \boldsymbol{h}_{\hat{\jmath}}\right\|_F^2, \quad \text{(B.19)}$$

where the vectors $\boldsymbol{h}_j$ and $\boldsymbol{h}_{\hat{\jmath}}$ are the j^{th} and $\hat{\jmath}^{th}$ columns of the channel matrix $\boldsymbol{H}$. The mathematical symbol $\|\cdot\|_F$ is the Frobenius norm.

Since we consider K-multiplicative i.i.d complex fading channels in this paper, this implies that the complex random L_r dimensional vectors $\boldsymbol{h}_j$ and $\boldsymbol{h}_{\hat{j}}$ have vector entries which are products of K complex standard Gaussian i.i.d random variables as shown in (B.1). There is no literature that currently has a closed form distribution of the product of K complex standard Gaussian i.i.d random variables. The next section deals with a proposed approximation method to find the unknown distribution of the random variable v for $K \geq 2$.

N.B: random variable v models the scaled square of the Euclidean distance between two column vectors of the channel matrix $\boldsymbol{H}$.

3.2.1 Distribution approximation of Q-function random parameter

Re-defining random variable v, (B.19) becomes

$$v \triangleq \frac{\overline{\gamma}}{2}\left|x_q\right|^2 R, \tag{B.20}$$

where $R = \left\|\boldsymbol{h}_j - \boldsymbol{h}_{\hat{j}}\right\|_F^2$.

Each entry of the L_r dimensional vectors $\boldsymbol{h}_j$ and $\boldsymbol{h}_{\hat{j}}$ is obtained from the product of K standard complex Gaussian random variables as shown in (B.1). Since no closed form distributions exist in current mathematics literature for the generic product of K standard complex Gaussian random variables, an algorithm is proposed to approximate the distribution of the random variable R. By generating the random data for R based on (B.20) for $K \geq 2$ via simulations, with a population size of 1000 000, it is found graphically that the envelope of the normalized histogram of this random data (R) follows a lognormal distribution. Algorithm 1, presented in this paper, merely determines the distribution parameters of the lognormal distribution by fitting the lognormal distribution, using maximum likelihood estimation, to the population of the random variable R.

Algorithm 1:

Step 1: Set the number of fading scenarios K.

Step 2: Set population size to N=1000 000.

Step 3: Set number of receive antennae $L_r = 4$, for a MIMO configuration with 4 receive antennae.

Step 4: Create *N* random variables as follows:

a) **:** Create **two** L_r-dimensional vectors which have entries derived from (B.1). The standard complex Gaussian random variables are generated by $\alpha = (randn(1) + 1j * randn(1))/\sqrt{2}$, where *j* in this case is a complex number.

b) **:** Find the value of the random variable R from the definition in (B.20) by finding the vector difference between these **two** L_r-dimensional vectors and computing the square of the Frobenius norm of the resultant vector difference.

c) **:** Save the result from Step (b) in an *N*-dimensional vector ***R_vec1***.

d) **:** Repeat Steps (a) to (c) until there are *N* random variables in vector ***R_vec1***.

Step 5: Fit a lognormal distribution to the random data in vector ***R_vec1*** using maximum likelihood estimation. This will determine the population mean μ_R and standard deviation σ_R of the underlying normal distribution of the lognormally distributed random variable *R*.

N.B: $randn(\cdot)$ is an inbuilt Matlab function for generating Gaussian random data.

Based on Algorithm 1, the population mean and standard deviation for the different *K* values are obtained and tabulated in Table B.1.

Table B.1: Population mean and standard deviation for different *K* values.

K	2	3	4	5	6	7	8	9	10
μ_R	1.85	1.71	1.53	1.32	1.08	0.83	0.56	0.27	-0.033
σ_R	0.70	0.88	1.06	1.23	1.39	1.53	1.67	1.81	1.94

In Table B.1, $K \geq 2$. This is because we consider a multiplicative complex fading channel in this paper. Based on the mean and standard deviation values tabulated in Table B.1, a lognormal distribution PDF graph can be plotted for each *K*. To validate the random variable *R* being lognormally distributed, a normalized histogram with $\sqrt{N}$ bins is plotted using the random data stored in vector ***R_vec1*** obtained from Algorithm 1, where *N* is the population size. The

lognormal distribution PDF graphs can be generated using the statistical values presented in Table B.1. The PDF graphs are overlaid onto the normalized histogram to compare the shape of both the approximate distribution and the actual distribution. For example, two graphs for *K=5* and *K=6* are presented in Fig. B.1 and B.2 that confirm that the random variable *R* is lognormally distributed according to the PDF

$$f(R) = \frac{1}{R\sigma_R\sqrt{2\pi}} e^{-\frac{(logR-\mu_R)^2}{2\sigma_R^2}}, \forall\, R > 0 \text{ [16, pp. 209-211]} \quad \text{(B.21)}$$

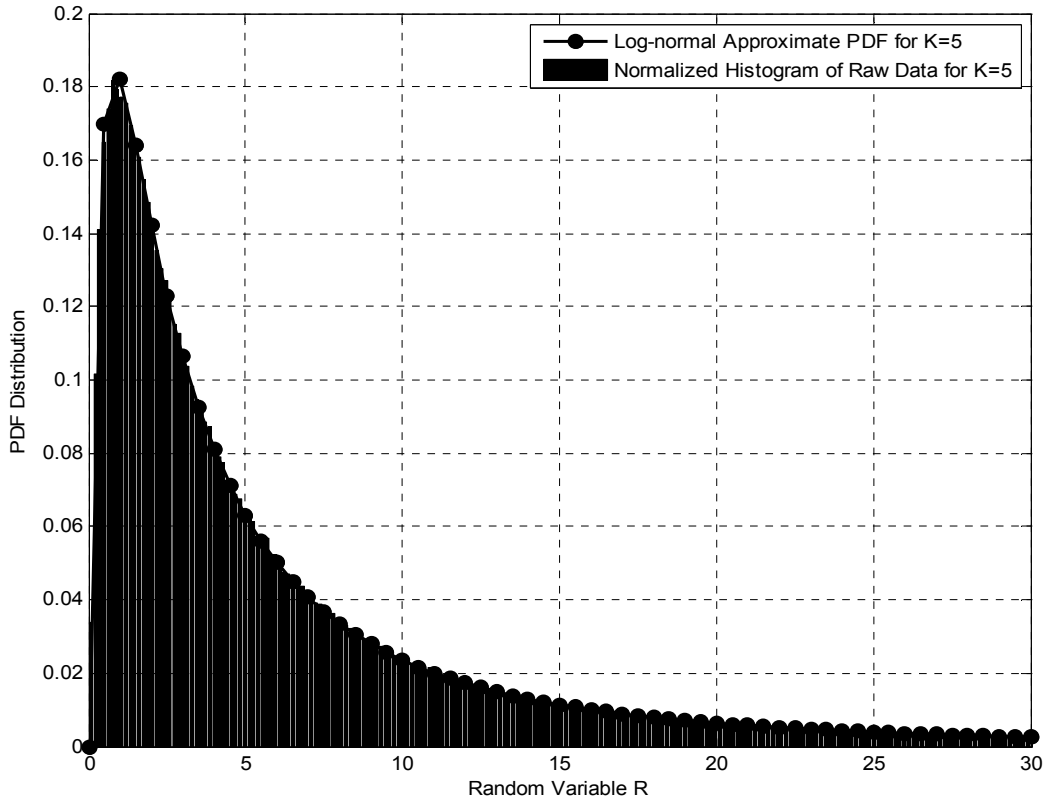

Fig. B.1 Lognormal PDF approximation versus normalized histogram random data for *K*=5

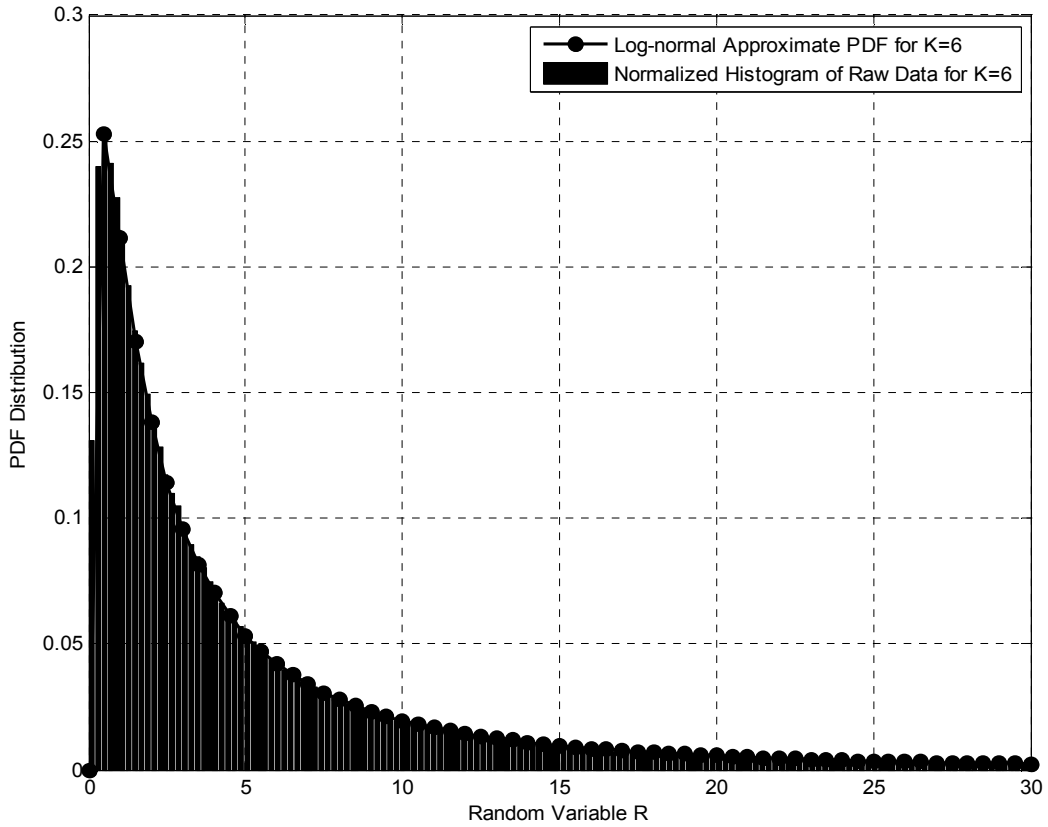

Fig. B.2 Lognormal PDF approximation versus normalized histogram random data for K=6

It is evident from these two graphs in Fig. B.1 and B.2 that a lognormal distribution is an appropriate distribution fit for the random variable R. A formal proof will follow using the Anderson-Darling goodness of fit test for normality [19] which will confirm that the parameters found by means of using Algorithm 1 are indeed valid.

NB: the number of histogram bins can be increased to generate a smooth histogram as shown in Fig. B.1 and B.2.

3.2.2 Anderson-Darling goodness of fit test

In the previous section, it was determined that the random variable R follows a lognormal distribution. Then depending on the value of K, for $K \in [2:10]$, lognormal distribution

population parameters were determined and tabulated in Table B.1. Though K is not upper-bounded, for purposes of presentation we restrict K up to 10 as it is impractical to find the distribution parameters for all possible K values. A formal proof is presented in this Section to a sample of n random data drawn from the population of R. This will validate the population parameters tabulated in Table B.1. Given the fact that the natural logarithm (*log*) of a lognormally distributed random variable is normally distributed [19], we can then perform a normality test to validate the population parameters determined by Algorithm 1. The following Algorithm is used to perform the Anderson-Darling goodness of fit test for normality [19]:

Algorithm 2:

Step 1: Set n=1000 samples, and also set K.

Step 2: State Null Hypothesis H_0: The sample **comes** from a Normal distribution $N(\mu_R, \sigma_R)$.

μ_R and σ_R are found in Table B.1 for each K value.

Step 3: State Alternative Hypothesis: H_1: The sample **does not** come from a Normal Distribution

Step 4: Perform test statistic computation as follows:

a) **:** Translate lognormally distributed random variable R to a normally distributed random variable *log(R).* This is implemented by taking the natural logarithm (*log)* of the n-dimensional vector ***R_vec2*** with random data R generated identically to Algorithm 1 with the exception of the sample size limit being n and not N.

b) **:** Standardize the normal random variables derived from Step (a) using

$$\boldsymbol{X} = \frac{log(\boldsymbol{R\_vec2}) - \mu_R}{\sigma_R}$$

c) **:** Sort in ascending order the random data in n-dimensional vector $\boldsymbol{X}$.

d) **:** Using the standard normal cumulative distribution function (CDF) for $\boldsymbol{X}$

$F(\boldsymbol{X}) = \frac{1}{2}\big(1 + 2Q(\boldsymbol{X})\big)$ [16], where $Q(\cdot)$ is the Q-function, and the Anderson-Darling test statistic, we compute A^2:

$$A^2 = -n - \left(\frac{1}{n}\right)\sum_{r=1}^{n}(2r-1)\left(log\left(F(\boldsymbol{X}_r)\right) + log\left(1 - F(\boldsymbol{X}_{n+1-r})\right)\right) \text{ [19]}$$

e) **:** Store test statistic values from Step (d) in vector ***A*.**

f) **:** Repeat Steps (a) to (e) until the number of elements in vector ***A*** is 100.

Step 5: Find the mean of the vector ***A*** and plot this mean value for each *K* value set in Step 1.

Step 6: Compare 5% significance level critical value of 2.492 to the mean test statistic value for a particular *K* value. Note that this test is a normality test with known normal distribution population parameters. Hence asymptotic critical values are used. Reject Null Hypothesis H_0 if mean test statistic is greater than the 5% significance level critical value of 2.492, otherwise accept it.

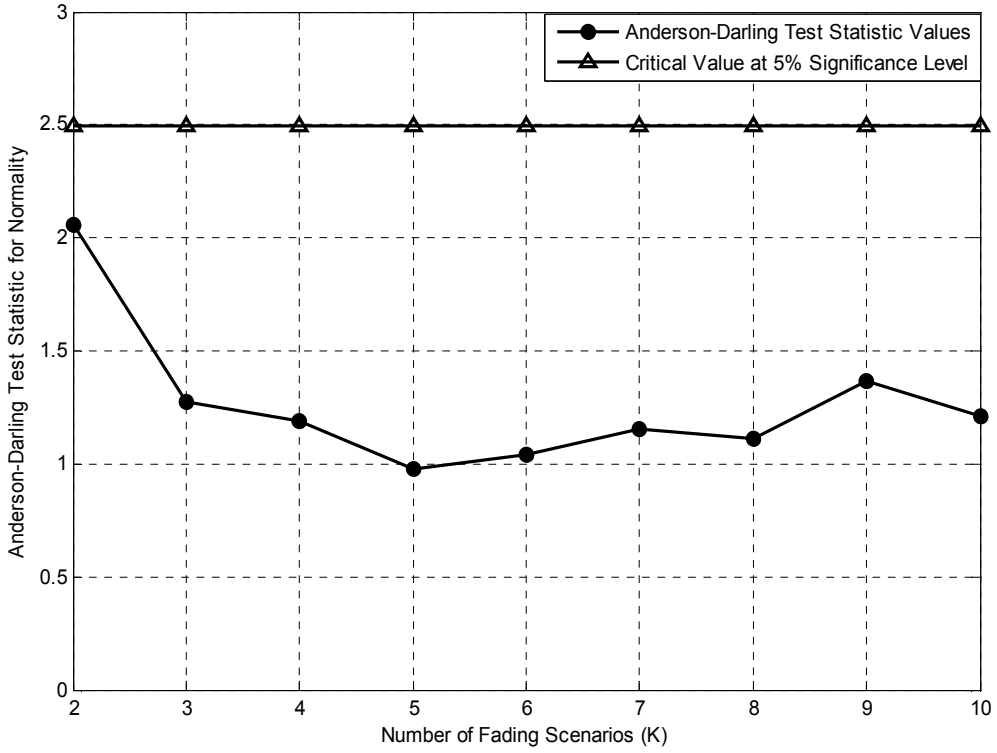

Fig. B.3 Anderson-Darling goodness of fit test graphical results for $K \in [2{:}10]$

Fig. B.3 exhibits the mean test statistics versus the 5% significance level critical value for each *K* value tabulated in Table B.1. It is evident that our approach is valid as the mean statistic for each *K* value is below the critical value which implies that the Null Hypothesis is accepted and hence for each *K* value parameters tabulated in Table B.1, we can conclude that the random variable *R* is lognormally distributed.

3.2.3 Pairwise error probability approximation

From the definition of the random variable *v* in (B.20), we can conclude that *v* is also lognormally distributed as random variable *v* is a multiple of the random variable *R*. Having established that fact, the parameters for the underlying normal distribution of the lognormal distribution of *v* need to be found. Using (B.20) and taking the natural logarithm of both sides of (B.20) we get

$$log(v) = log\left(\frac{\bar{\gamma}}{2}\left|x_q\right|^2 R\right) = log\left(\frac{\bar{\gamma}}{2}\left|x_q\right|^2\right) + log(R), \tag{B.22}$$

By letting $\varphi = \frac{\bar{\gamma}}{2}\left|x_q\right|^2$ and knowing that $log(R)$ is normally distributed. This implies that $log(v)$ is also normally distributed. By evaluating the mean and variance of both sides of (B.22) and using the properties that $E(f) = f$ and $Var(f) = 0$, where f is a constant and $E(\cdot)$ is the expectation and $Var(\cdot)$ is the variance, then it can be shown that

$$\sigma_v = \sigma_R \text{ and } \mu_v = log(\varphi) + \mu_R, \tag{B.23}$$

where σ_v is the standard deviation of $log(v)$ and μ_v is the mean of $log(v)$.

Hence the lognormal distribution for the random variable *v* is defined using the PDF

$$f(v) = \frac{1}{v\sigma_v\sqrt{2\pi}} e^{-\frac{(logv-\mu_v)^2}{2\sigma_v^2}}, \forall\, v > 0 \quad \text{[16, pp. 209-211]} \tag{B.24}$$

The PEP stated in (B.18) is a random variable dependent on the lognormally distributed random variable *v*. In order to find the average PEP, the expression in (B.25) needs to be evaluated

$$P\left(\boldsymbol{x}_{jq} \to \boldsymbol{x}_{\hat{j}q}\right) = \int_0^\infty Q\left(\sqrt{v}\right) f(v) dv, \tag{B.25}$$

where $f(v)$ is defined in (B.24).

Based on the definition of the Q-function in (B.18) we have $Q\left(\sqrt{v}\right) = \frac{1}{\pi}\int_0^{\pi/2} e^{-v/2\sin^2\theta}d\theta$. Let $s = (1/2\sin^2\theta)$ then (B.25) becomes

$$P\left(\boldsymbol{x}_{jq} \to \boldsymbol{x}_{\hat{j}q}\right) = \frac{1}{\pi}\int_0^{\pi/2}\int_0^{\infty} e^{-sv} f(v)\, dv d\theta, \tag{B.26}$$

In (B.26), we define $M(v) \triangleq \int_0^{\infty} f(v)e^{-sv}\, dv$ as the Moment Generating Function (MGF) of a lognormally distributed random variable *v*. Since there is no closed form solution for the MGF of a lognormally distributed random variable, the authors in [17] propose an accurate approximation for evaluating the MGF. The technique of Gauss-Hermite quadrature is employed by [17] to find the MGF approximation. We apply the same technique to find $M(v)$ as follows:

Substituting (B.24) into MGF $M(v)$, $M(v) = \int_0^{\infty} e^{-sv}\frac{1}{v\sigma_v\sqrt{2\pi}} e^{-\frac{(\log v-\mu_v)^2}{2\sigma_v^2}}\, dv$ by letting

$t = \frac{(\log v-\mu_v)}{\sqrt{2}\sigma_v}$ and based on the technique of Gauss-Hermite quadrature, $M(v)$ becomes

$$M(v) = \sum_{l=1}^{L}\frac{\omega_l}{\sqrt{\pi}} e^{-\left(se^{(\sqrt{2}\sigma_v a_l+\mu_v)}\right)} + R_L, \tag{B.27}$$

where R_L decreases rapidly as *L* increases. We can assume that for *L*=10, R_L is negligible. ω_l and a_l are the *L*-order Hermite polynomial weights and zeroes tabulated in [18, Tbl. 25.10] for *L*=10, respectively.

Since R_L is negligible when *L*=10, we can eliminate it from (B.27) and substitute the resulting approximation into (B.26) and get

$P\left(\boldsymbol{x}_{jq} \to \boldsymbol{x}_{\hat{j}q}\right) \approx \frac{1}{\pi}\int_0^{\pi/2}\sum_{l=1}^{L}\frac{\omega_l}{\sqrt{\pi}} e^{-\left(se^{(\sqrt{2}\sigma_v a_l+\mu_v)}\right)} d\theta$, substituting back $s = (1/2\sin^2\theta)$ and re-arranging and letting $A_l = \frac{\omega_l}{\sqrt{\pi}}$ and $B_l = e^{(\sqrt{2}\sigma_v a_l+\mu_v)}$ we get

$$P\left(\boldsymbol{x}_{jq} \to \boldsymbol{x}_{\hat{j}q}\right) \approx \frac{1}{\pi}\sum_{l=1}^{L} A_l \int_0^{\pi/2} e^{-B_l/2\sin^2\theta} d\theta, \tag{B.28}$$

Using the definition of the Q-function in (B.18) we deduce that $Q\left(\sqrt{B_l}\right) = \frac{1}{\pi}\int_0^{\pi/2} e^{-B_l/2\sin^2\theta} d\theta$, hence (B.28) simplifies to

$$P(\boldsymbol{x}_{jq} \rightarrow \boldsymbol{x}_{\hat{j}q}) \approx \sum_{l=1}^{L} A_l Q(\sqrt{B_l}), \tag{B.29}$$

Since an approximate expression has been found for the average PEP, the upper bound bit error probability for the transmit antenna index estimation is given in (B.30) by substituting (B.29) into (B.17) and getting

$$\overline{BER}_a(\bar{\gamma}) \leq \frac{\sum_{j=1}^{L_t} \sum_{q=1}^{M} \sum_{\hat{j}=1}^{L_t} N(j,\hat{j}) \sum_{l=1}^{L} A_l Q(\sqrt{B_l})}{L_t M}, \tag{B.30}$$

where $\sigma_v = \sigma_R,\ \mu_v = log(\varphi) + \mu_R$ and $\varphi = \frac{\bar{\gamma}}{2}|x_q|^2$. σ_R and μ_R are found from Algorithm 1 for each K value. For $K \in [2:10]$ the values are readily available in Table B.1. Thus the transmit antenna index estimation upper bound BER in (B.30) together with the symbol estimation BER approximation in (B.15) are substituted into (B.3) to determine the overall analytical lower bound BER for SM over multiplicative fading channels.

4 Simulation Results

In this Section, we use 2×4 and 4×4 MIMO configurations, with $K \in [5:6]$ fading scenario's per channel, as examples to validate the analytical frameworks developed in Section 3 by comparing the analytical BER performance of the transmitted symbol estimation and transmit antenna estimation to that of the simulated BER over multiplicative complex fading channels. The parameters regarding the AWGN and fading channel are consistent with those defined in Section 2. The following were assumed during simulation: Gray coded MQAM constellation, block size is set to $N_b = 1080$ bits, transmit and receive antennae are separated wide enough to avoid correlation and the total transmit power is the same for all transmissions.

4.1 Analytical and simulated BER of symbol estimation

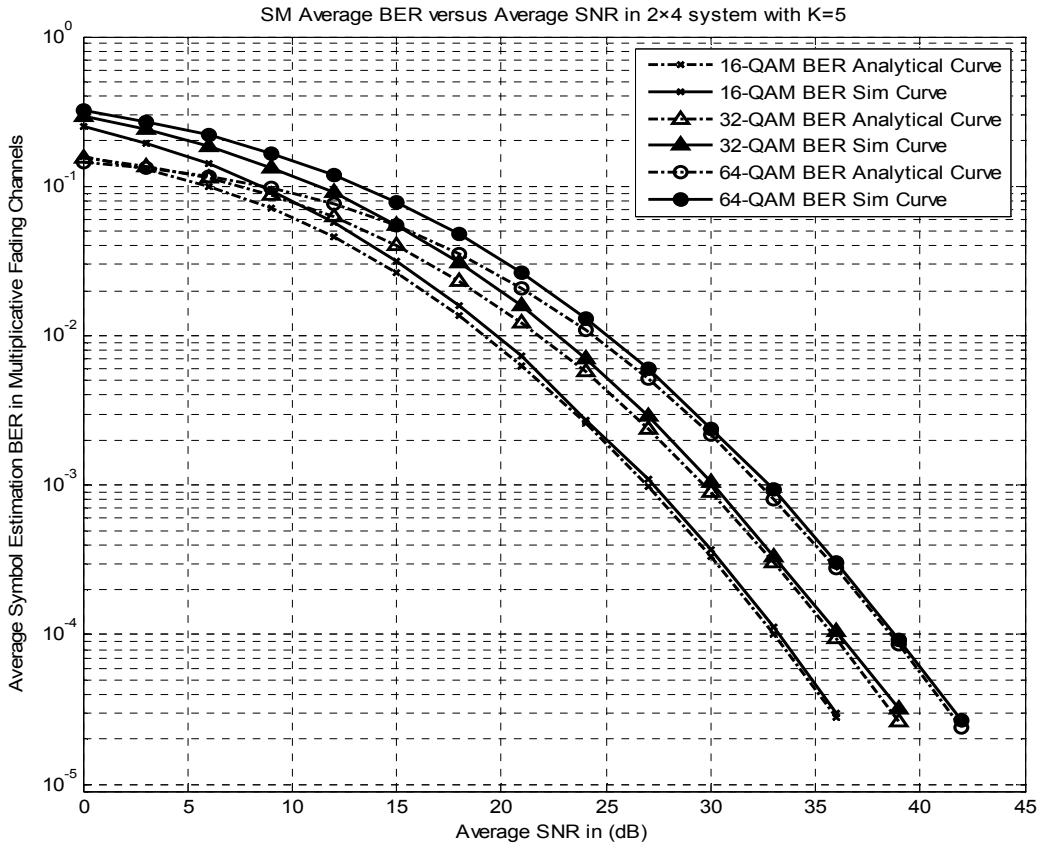

Fig. B.4 BER performance of symbol estimation for 2 × 4 16, 32 and 64-QAM when K=5.

Fig. B.4 shows BER performance of transmitted symbol estimation for 2 × 4 16, 32 and 64-QAM over K=5 multiplicative complex fading wireless channels. From Fig. B.4, it is found that the analytical BER of the transmitted symbol estimation in (B.15) is accurate at high average SNR and inaccurate at low average SNR as a result of the assumption made of a symbol error being caused by only 1 bit error at a time. This assumption does not hold at low average SNR as more bit errors than 1 can occur at a time.

4.2 Analytical and simulated BER of antenna estimation

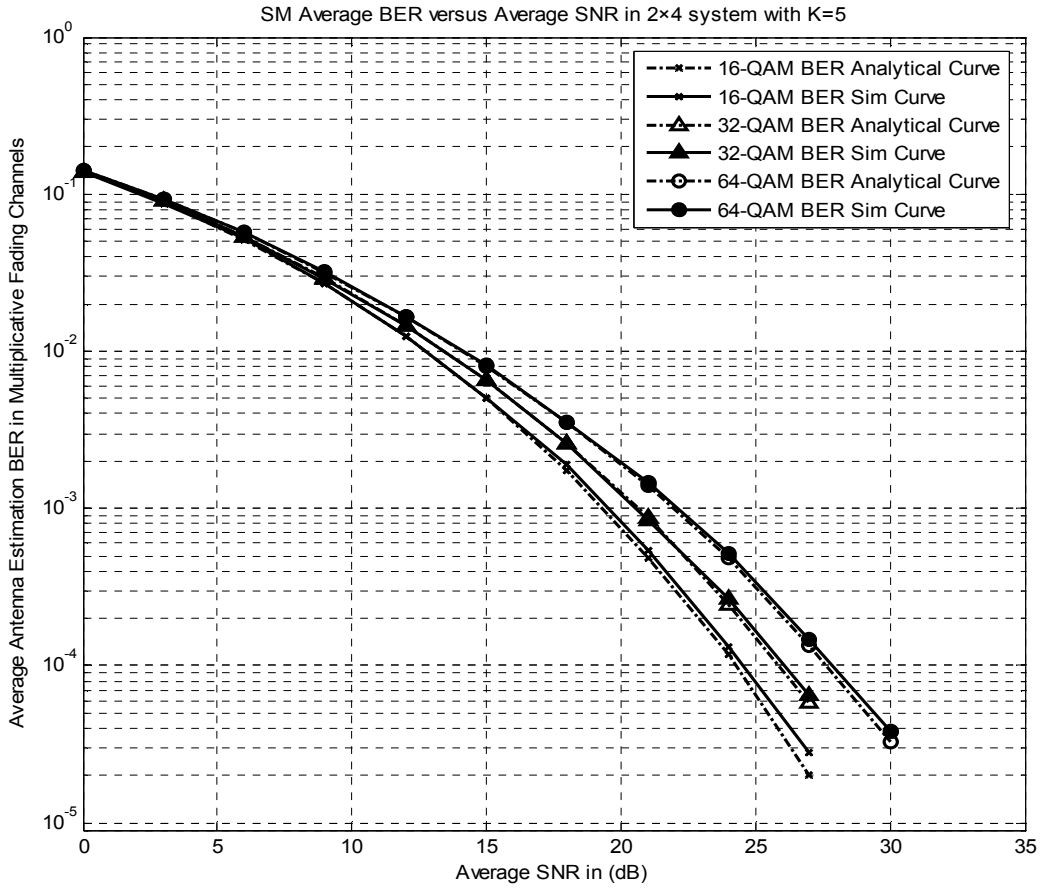

Fig. B.5 BER performance of transmit antenna index estimation for 2 × 4 16, 32 and 64-QAM when K=5.

Fig. B.5 shows the BER performance of transmit antenna index estimation for 2 × 4 16, 32 and 64-QAM over K=5 multiplicative complex fading wireless channels. The analytical BER of transmit antenna estimation defined in (B.30) is validated by Monte-Carlo simulation results. The BER of transmit antenna estimation is slightly loose at high average SNR for 16-QAM. Since the BER of transmit antenna estimation is derived using two approximations namely: the Gauss-Hermite quadrature approximation for the MGF integral and the log normal distribution approximation proposed in this paper, it is natural for inaccuracies to manifest themselves in the analytical BER performance of transmit antenna estimation. Looseness of the analytical BER

upper bound of transmit antenna index estimation relative to simulation BER can occur as a result of compound inaccuracies due to the two approximations.

4.3 Analytical and simulated BER of MQAM SM over multiplicative complex fading channels

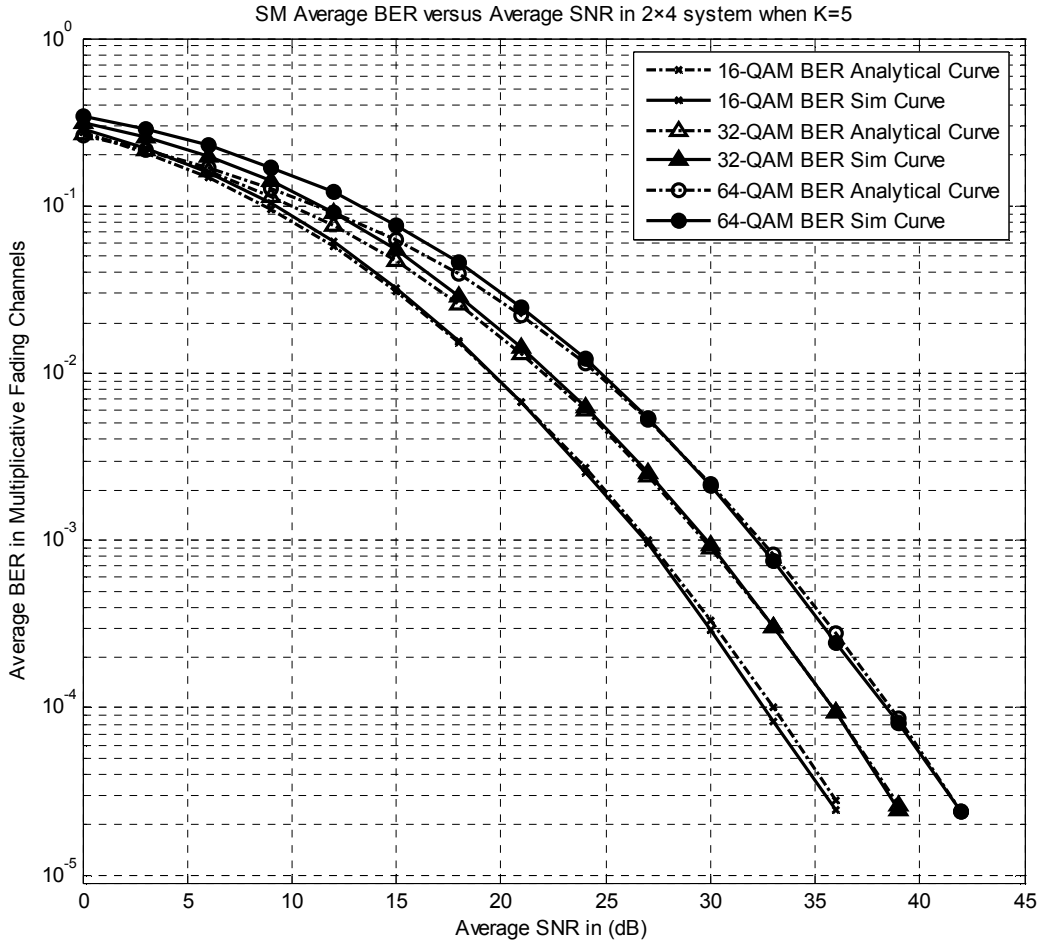

Fig. B.6 BER performance of 2 × 4 16, 32 and 64-QAM when K=5.

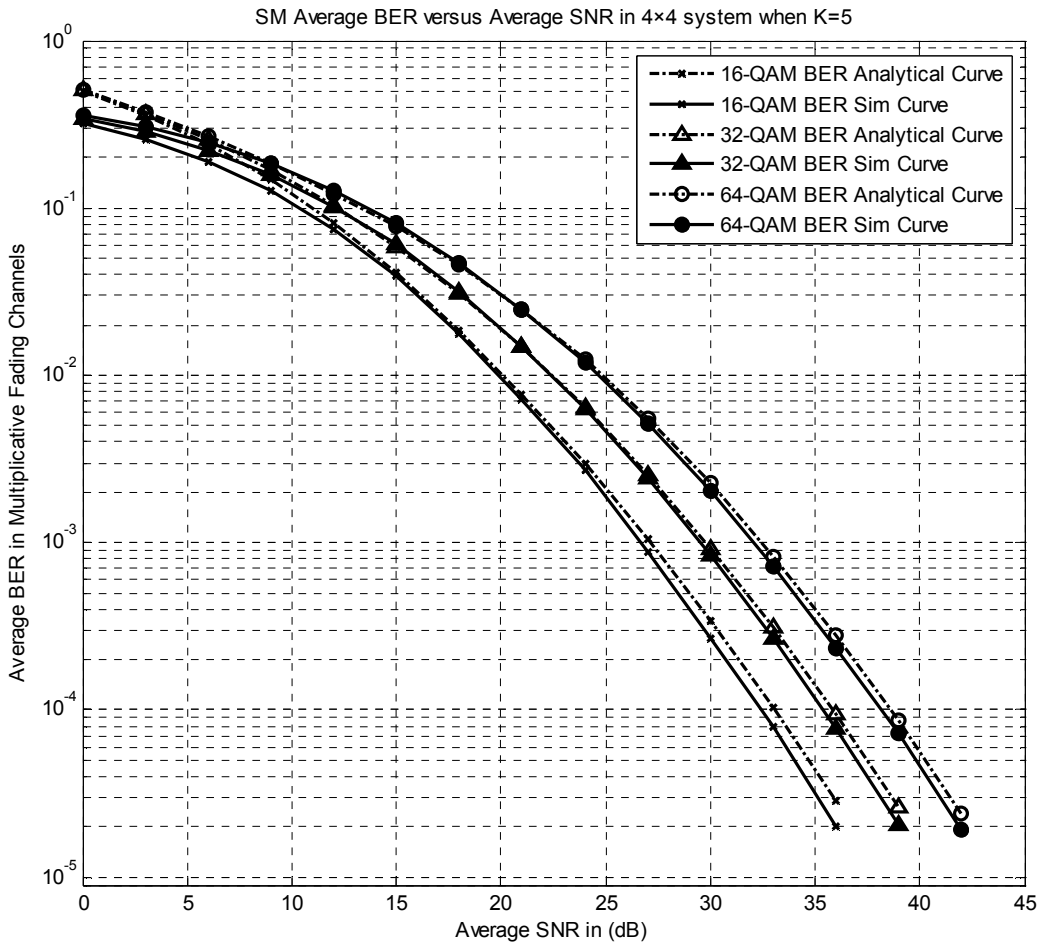

Fig. B.7 BER performance of 4×4 16, 32 and 64-QAM when K=5.

Fig. B.6 and B.7 shows the BER performance of SM for 2×4 and 4×4 MQAM over $K = 5$ multiplicative complex fading wireless channels, respectively. The results in Fig. B.6 and B.7 prove the fact that the SM simulated BER over $K = 5$ multiplicative complex fading channels can be predicted using the analytical BER expression in (B.3) for different $L_t \times L_r$ MIMO configurations. The analytical error performance lower bound of SM over 4×4 wireless channels is tightened relative to the simulation error performance by assuming that the receiver node always estimates the transmit antenna index with the closest spatial constellation to that of the active transmit antenna index. The closest spatial constellation is defined as that constellation which has a maximum Hamming distance of unity relative to the active transmit antenna index

spatial constellation. However, despite tightening the error performance lower bound of SM over 4×4 wireless channels, the bound is slightly loose at high average SNR as a result of the looseness of the BER upper bound of transmit antenna index estimation at high average SNR. This looseness of the BER lower bound of SM is more prevalent when using lower modulation orders for symbol transmission (i.e $M \rightarrow L_t$). As seen in Fig. B.7, as the modulation order increases from 16 to 64-QAM, the BER lower bound becomes tighter. This is because as the modulation order (M) increases relative to the spatial constellation size (L_t), the BER of symbol estimation dominates in the BER performance of SM.

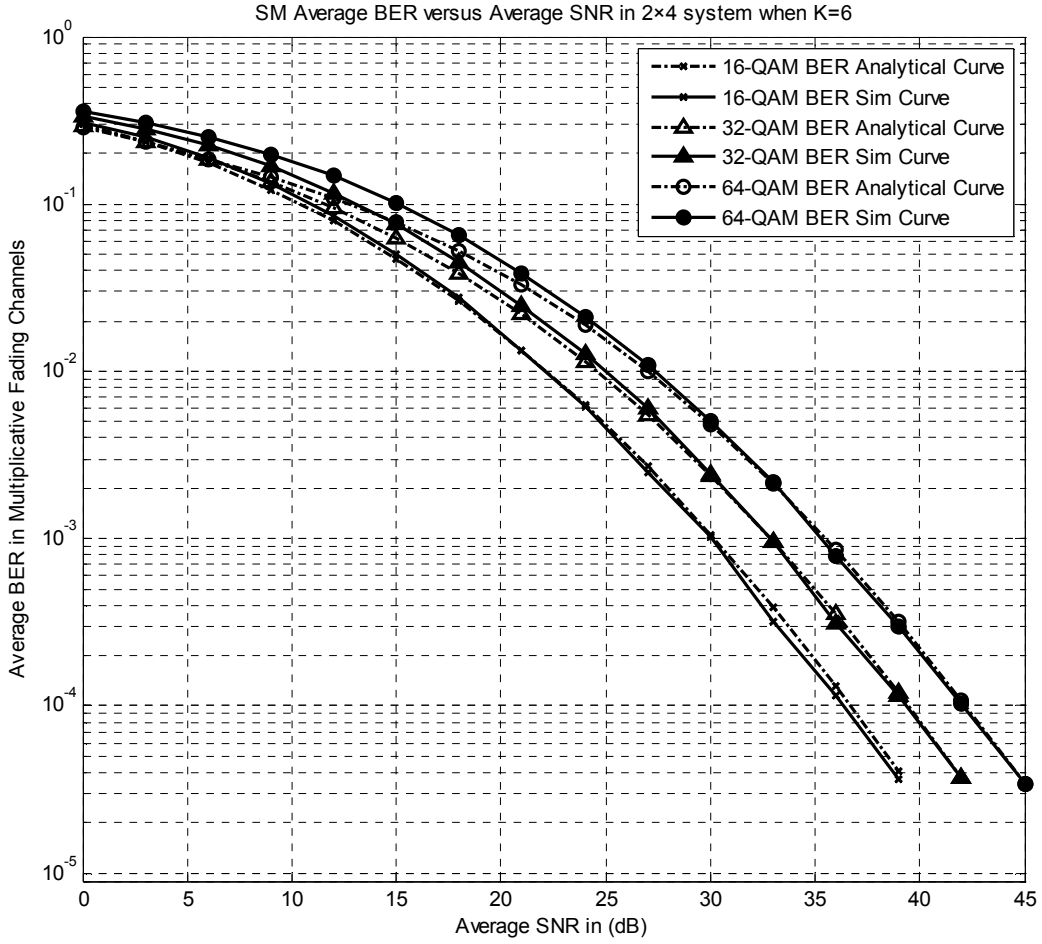

Fig. B.8 BER performance of 2×4 16, 32 and 64-QAM when *K*=6.

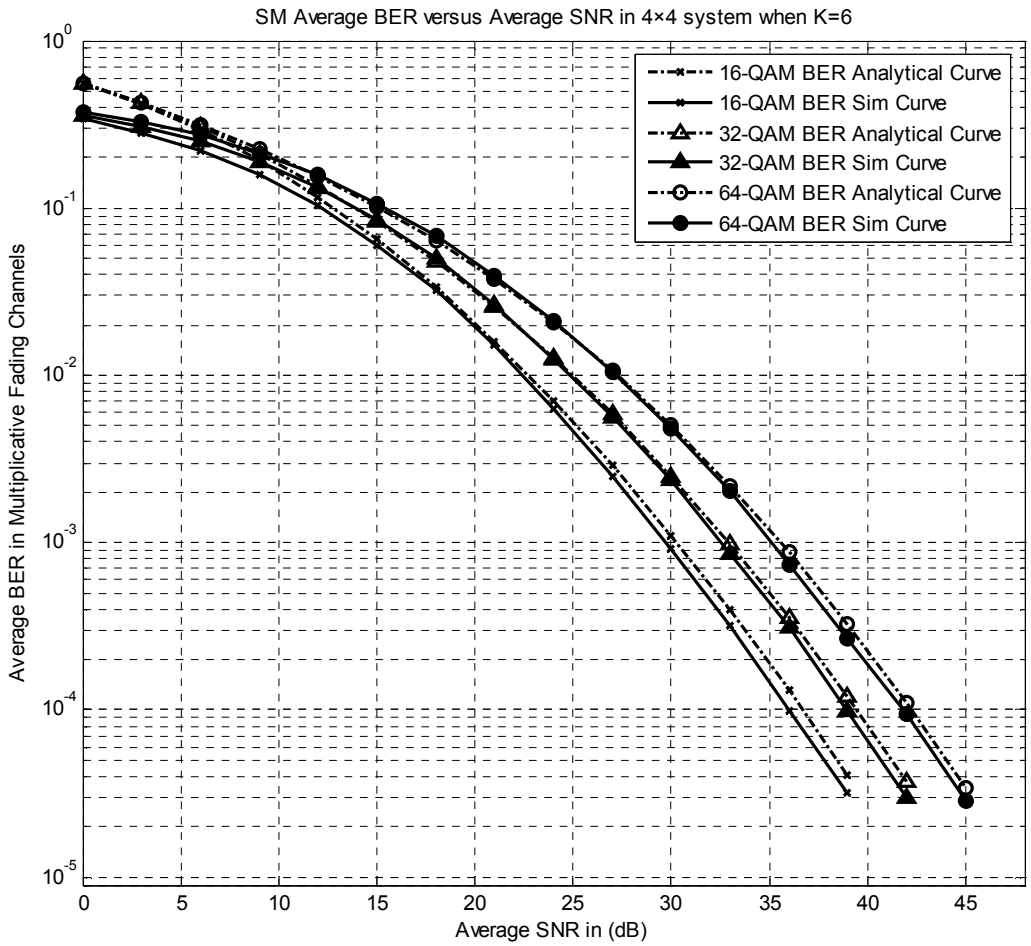

Fig. B.9 BER performance of 4 × 4 16, 32 and 64-QAM when *K*=6.

Fig. B.8 and B.9 shows the BER performance of SM for 2 × 4 and 4 × 4 MQAM over *K*=6 multiplicative complex fading wireless channels, respectively. The results in Fig. B.8 and 9 also prove the fact that the expression in (B.3) can closely predict the BER performance over *K*=6 multiplicative complex fading wireless channels. These results shown in Fig. B.6 to B.9 further validate the distribution approximation Algorithm proposed in Section 3.2.1. A further observation is made in Fig. B.6 to B.9 that the BER performance worsens as the number of fading scenarios (*K*) increase. This is expected as increasing the number of independent fading scenarios between a transmit antenna and receive antenna path, increases the likelihood of deep fades occurring in that wireless channel path. Another observation is that, as the number of

transmit antennae is increased from 2 to 4, the BER performance is negligibly affected. This may be due to the fact that as the number of fading scenarios become large, $K \rightarrow \infty$, they become the dominant factor in BER performance degradation as opposed to the number of transmit antennae in the MIMO configuration.

5 Conclusion

We apply SM over multiplicative complex fading wireless channels. The analytical BER approximations derived in this paper are validated by Monte-Carlo simulation results. The results show agreement under different MIMO configurations and also under a different number of K i.i.d fading scenarios. The lognormal distribution approximations developed in this paper for different K fading scenarios are validated by the Anderson-Darling goodness of fit test at the 5% significance level, hence the lognormal distribution population parameters tabulated in Table B.1, for different K fading scenarios, can be used directly in future studies concerning SM over multiplicative complex fading channels. The analytical BER approximations derived in this paper are restricted to multiplicative fading environments with $K \geq 2$ and SM that uses modulation orders that are much greater than the spatial constellation size (i.e $M \gg L_t$). The BER for the special case, when $K = 1$, cannot be deduced from our BER approximations as our distribution approximation assumes that random variable v is lognormally distributed. This is not the case for the $K = 1$ scenario as the random variable v is analytically shown by [3] to be Chi-Squared distributed.

References

[1]. R.Y. Mesleh, H. Haas, C.W. Ahn, S. Yun, "Spatial modulation-a new low complexity spectral efficiency enhancing technique", *First international conference on communications and networking in China*, 2006.

[2]. P. Wolniansky, G. Foschini, G. Golden and R. Valenzuela, "V-BLAST: An Architecture for Realizing very High Data Rates over the Rich- Scattering Wireless Channel", in *Proc URSI Int. Symp. on Signals , Systems and Electronics (ISSSE '98.)*, Pisa, pp. 295–300, 1998.

[3]. N.R. Naidoo, H. Xu, T. Al-Mumit Quazi, "Spatial modulation: optimal detector asymptotic performance and multiple-stage detection", *IET proceedings Communications,* vol. 5, no. 10, pp. 1368-1376, July 2011.

[4]. F. Babich and G. Lombardi, "Statistical analysis and characterization of the indoor propagation channel", *IEEE Trans. on Comms,* vol. 48, no. 3, pp. 455-464, March 2000.

[5]. F. Hansen and F. I. Meno, "Mobile fading-Rayleigh and lognormal superimposed", ", *IEEE Trans. Veh. Technol.*, vol. 26, no.4, pp. 332-335, November 1977.

[6]. J.B. Andersen and I.Z. Kovács, "Power distribution revisited", *in Proc. COST273 3rd Management Committee Meeting*, Guilford, U.K., 2002.

[7]. N.H. Tran, H.H. Nguyen, T. Le-Ngoc, "Application of signal space diversity over multiplicative fading channels", *IEEE Signal Processing Letters,* vol. 16, no. 3, pp. 204-207, March 2009.

[8]. G.K. Karagiannidis, N.C. Sagias, P.T. Mathiopoulos, "N*Nakagami: A Novel Stochastic Model for cascaded fading channels*", IEEE Trans. on Comms,* vol. 55, no. 8, pp. 1453-1458, August 2007.

[9]. J. Salo, H.M. El-Sallabi, P. Vainikainen, "The distribution of the product of independent Rayleigh random variables", *IEEE Trans. on Antennae and propagation,* vol. 54, no. 2, pp. 639-643, February 2006.

[10]. I.S. Gradshteyn, I.M. Rhyzik, "Table of Integrals, Series and Products", *Academic Press (Elsevier)*, 7th Edition, 2007.

[11]. R.Y. Mesleh, H. Haas, S. Sinanovic, C.W. Ahn, S. Yun, "Spatial Modulation", *IEEE Trans. Veh. Technol.*, vol. 57, no.4, pp. 2228-2241, July 2008.

[12]. M.K. Simon, M.S. Alouini, "Digital Communication over fading channels", *New York: John Wiley*, 1st Edition, 2000.

[13]. E. Kreyszig, "Advanced Engineering Mathematics", *John Wiley and Sons*, 7th Edition, 1993.

[14]. J.G. Proakis, "Digital Communications", *New York: McGraw-Hill*, 4th Edition, 2001.

[15]. J. Jeganathan, A. Ghrayeb, L. Szczecinski, A. Ceron, "Space shift keying modulation for MIMO channels", *IEEE Trans. on Wireless Comms.*, vol. 8, no. 7, pp. 3692-3703, July 2009.

[16]. T.T. Soong, "Fundamentals of probability and statistics for engineers", *John Wiley and Sons*, 2004.

[17]. N.B. Mehta, A.F. Molisch, "Approximating a Sum of Random variables with a Lognormal", *IEEE Trans. on Wireless Comms.*, vol. 6, no. 7, pp. 2690 – 2699, July 2007.

[18]. M. Abramowitz and I. Stegun, "Handbook of mathematical functions with formulas, graphs, and mathematical tables", *Dover*, 9th Edition, 1972.

[19]. R.B. D'Agostino, M.A. Stephens, "Goodness of Fit Techniques", *Marcel Dekker, New York*, June 1986.

[20]. J. Jeganathan, A. Ghrayeb, L. Szczecinski, "Spatial modulation: optimal detection and performance analysis", *IEEE Commun. Lett.,* vol. 12, no. 8, pp. 545-547, August 2008.

Part III

Conclusion

1 Conclusion

Constant power adaptive modulation is a technique used in this study to improve the average throughput in a conventional SM scheme, subject to a target BER constraint. It improves the average throughput by adapting the modulation order based on the quality of the received SNR. A-QASM ensures that the highest possible data transmission rate is chosen for a particular channel quality. The received SNR plays an important role in an A-QASM scheme, as it defines the wireless channel quality, and hence, this study makes effort to define it.

SM is a low complexity MIMO scheme that can be implemented in small mobile devices e.g cellular phones. This will allow small mobile devices to achieve high data rate transmissions, link reliability and thus improve system throughput. However, transmission over a wireless medium with a constrained BER is only possible if an analytical BER expression exists for that specific wireless channel model. This study derives a BER lower bound approximation for SM over cascaded/multiplicative fading channels. The study exhibits the results in two papers contained in this dissertation.

In Paper A, the analytical BER lower bound of A-QASM closely agrees with the Monte Carlo simulation results. The study also shows via simulation that the average throughput of SM transmission is improved by applying constant power adaptive modulation to SM. This study also shows that the proposed definitions for the received SNR are interchangeable, as both definitions yield similar A-QASM BER and throughput performances, under the assumption of perfect CSI.

In Paper B, the analytical BER lower bound of SM over cascaded/multiplicative fading channels is validated via Monte Carlo simulation for modulation orders much greater than the spatial constellation size (i.e $M \gg L_t$). The lognormal distribution approximation for the stochastic parameter with an unknown distribution is validated as an appropriate distribution fit by the Anderson-Darling goodness of fit test at the 5% significance level.